


General Rules for the Impact of Energetic Disorder and Mobility on Nongeminate Recombination in Phase-Separated Organic Solar Cells

Guangzheng Zuo¹, Safa Shoaee¹, Martijn Kemerink^{2,*} and Dieter Neher^{1,†}

¹*Institute for Physics and Astronomy, University of Potsdam, 14476 Potsdam-Golm, Germany*

²*Centre for Advanced Materials, Ruprecht-Karls-Universität Heidelberg, 69120 Heidelberg, Germany*

 (Received 2 July 2021; accepted 26 August 2021; published 15 September 2021)

State-of-the-art organic solar cells exhibit power conversion efficiencies of 18% and above. These devices benefit from the suppression of free charge recombination with regard to the Langevin limit of charge encounter in a homogeneous medium. It is recognized that the main cause of suppressed free charge recombination is the reformation and resplitting of charge-transfer (CT) states at the interface between donor and acceptor domains. Here, we use kinetic Monte Carlo simulations to understand the interplay between free charge motion and recombination in an energetically disordered phase-separated donor-acceptor blend. We identify conditions for encounter-dominated and resplitting-dominated recombination. In the former regime, recombination is proportional to mobility for all parameters tested and only slightly reduced with respect to the Langevin limit. In contrast, mobility is not the decisive parameter that determines the nongeminate recombination coefficient, k_2 , in the latter case, where k_2 is a sole function of the morphology, CT and charge-separated (CS) energetics, and CT-state decay properties. Our simulations also show that free charge encounter in the phase-separated disordered blend is determined by the average mobility of all carriers, while CT reformation and resplitting involves mostly states near the transport energy. Therefore, charge encounter is more affected by increased disorder than the resplitting of the CT state. As a consequence, for a given mobility, larger energetic disorder, in combination with a higher hopping rate, is preferred. These findings have implications for the understanding of suppressed recombination in solar cells with nonfullerene acceptors, which are known to exhibit lower energetic disorder than that of fullerenes.

DOI: [10.1103/PhysRevApplied.16.034027](https://doi.org/10.1103/PhysRevApplied.16.034027)

I. INTRODUCTION

The power conversion efficiency of organic solar cells (OSCs) has considerably improved over the past years, now surpassing 18% [1–5]. Due to the introduction of highly absorbing nonfullerene acceptors (NFAs), the short-circuit current density, J_{SC} , of such cells now approaches the values delivered by more traditional semiconductors of comparable band gap. Still, OSCs lag behind in terms of the open-circuit voltage, V_{OC} , and the fill factor, FF; the latter is determined by the competition between free charge extraction and recombination. It is well documented that free charge recombination, also denoted as nongeminate recombination, NGR, in organic solar cells is of second-order nature [6]:

$$R = k_2 n_e n_h = k_2 n_{CS}^2. \quad (1)$$

Here, R is the volume recombination rate; k_2 is the second-order NGR coefficient; and n_e and n_h are the density of free

electrons and holes, respectively. For intrinsic semiconductors, $n_e = n_h \equiv n_{CS}$ is the density of charge-separated states. For bimolecular free charge recombination, competition between charge extraction and recombination can be described by analytical “figures of merits” (FOMs) [7], one of which is as follows:

$$\alpha^2 = \frac{q^2 k_2 G d^4}{4 \mu_e \mu_h (k_B T)^2}. \quad (2)$$

Here, q is the elementary charge, G is the volume photogeneration rate, and d is the active-layer thickness. μ_e and μ_h are the electron and hole mobility, respectively, and $k_B T$ is the thermal energy. For $\alpha < 1$ the J - V characteristics can be approximated by the traditional Shockley diode equation, while the photocurrent becomes transport limited for $\alpha > 1$ [7]. Therefore, strategies to reduce $k_2/\mu_e \mu_h$ are desirable and form the motivation for this work.

In the simplest case of encounter-dominated recombination in a homogenous medium, NGR is described by the Langevin recombination coefficient (k_L):

$$k_2 = k_L \equiv q(\mu_e + \mu_h)/\epsilon_0 \epsilon_r, \quad (3)$$

*martijn.kemerink@cam.uni-heidelberg.de

†neher@uni-potsdam.de

rendering k_2 proportional to the sum of electron and hole mobilities. Here, ϵ_0 and ϵ_r are the vacuum and relative dielectric constants, respectively. The k_2 value of bulk-heterojunction (BHJ) OSCs is generally much smaller, corresponding to more than 100 times suppression of recombination compared with the Langevin limit in some extreme cases [8–15]. Such BHJ donor-acceptor blends ideally consist of extended domains of neat donor and acceptor components. It is proposed that stabilization of free charges on these domains reduces the rate through which oppositely charged free carriers meet at the donor-acceptor interface [15–17]. As outlined below, earlier kinetic Monte Carlo (KMC) simulations showed that phase separation is not sufficient to explain the highly suppressed recombination found in some BHJ OSCs [17,18]. In 2015, Burke *et al.* proposed that NGR was the consequence of efficient resplitting of CT states into free charges [19]. In this picture, free charge recombination results in the formation of interfacial CT states, which either decay back to the ground state or redissociate into free carriers (Fig. 1). Because the CT dissociation rate itself is a function of carrier mobility, the direct proportionality between k_2 and μ , as in the Langevin limit, may not hold true anymore. Another feature of the OSC's active layer is intrinsic energetic disorder. Energetic disorder is known to slow down carrier motion and to lead to transient (dispersive) phenomena. Various theoretical experimental works have studied the effect of disorder on characteristic photovoltaic parameters or on the dispersive recombination of free

charges [20–28]. In most of these studies, the focus was on the interrelation between characteristic of the recombination process parameters and the shape of the DOS (exponential or Gaussian) or the predominant recombination pathway. Fewer studies dealt with the interplay between free charge motion and recombination. An elegant analytical approach to relate these two processes was developed by Orenstein and Kastner [20,29]. These authors assume that charges move by thermal excitation to states at a transport energy of E_{tr} and that charges situated in the tail of the inhomogeneously broadened DOS must be excited back to that transport energy to be able to meet the countercharge. Since trapping and detrapping also govern the drift of carriers in an electric field, recombination and mobility are expected to follow similar dependencies on time and temperature and carrier density [30]. However, these and related theoretical approaches are applicable only to homogeneous media. The groups of Grove [17] and later Heiber [18] applied KMC to relate carrier transport in a phase-separated morphology to encounter-limited recombination. For the simplest case of balanced mobilities, the encounter-limited NG recombination rate is shown to be proportional to k_L and only slightly reduced (by no more than 50%) compared with the Langevin limit. Interestingly, energetic disorder has only a weak effect on the suppression of encounter-limited recombination in a phase-separated morphology, despite its large influence on charge carrier mobility. Very recently, Coropceanu *et al.* studied the transient NGR in phase-separated donor-acceptor blends

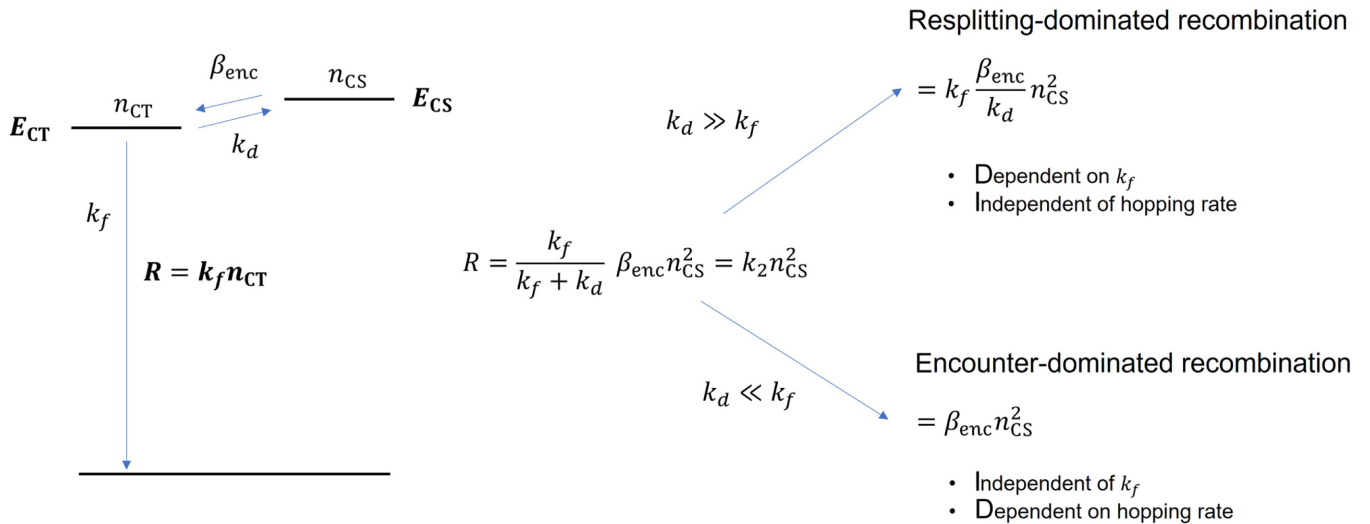


FIG. 1. Scheme showing the states involved in free charge recombination. Here, n_{CS} and n_{CT} are the density of free carriers (charge-separated states) and charge-transfer states, respectively; β_{enc} is the coefficient for bimolecular free charge encounter forming the CT state; k_d is the rate coefficient for CT dissociation into free charges; and k_f is the rate coefficient for the decay of the CT state to the ground state. Also depicted are the two extremes. For $k_d \ll k_f$, resplitting of the CT state is very unlikely, and the recombination rate, R , is determined by the encounter rate, which is independent of the CT decay rate but proportional to the carrier-hopping rate and with this to the carrier mobility. In contrast, if $k_d \gg k_f$, CT states resplit at a much higher rate than they decay to the ground state. Because β_{enc} and k_d depend linearly on the hopping rate, v_0 , its effect on the recombination rate cancels out while, on the other hand, R becomes strictly proportional to k_f .

under explicit consideration of CT formation, resplitting, and decay [31]. This study showed a significant attenuation of R with increasing disorder and CT lifetime, but no correlation to the carrier mobility was made.

Here, we perform KMC simulations of free carrier recombination in disordered phase-separated blends. By varying the attempt-to-hop frequency, ν_0 , and the energetic disorder, σ , over a wide range, we evaluate in detail the interplay between free charge carrier motion and recombination. Doing these simulations in a transient fashion, we gain access to the extraction-recombination balance as a function of the mean energy of the free carriers, down to the equilibrium situation. For low ν_0 , recombination is encounter dominated and proportional to the Langevin recombination rate, although it is reduced by a geometric reduction factor, which is nearly independent of energetic disorder. Increasing ν_0 causes a transition to the resplitting-dominated regime, where CT exciton dissociation competes efficiently with its decay to the ground state. Importantly, in this regime, the NGR coefficient becomes independent of ν_0 and, for a given energetic disorder, independent of μ . Here, k_2 is given only by the details of the energetics and morphology of the blend. Our simulations also show that the formation of a CT exciton in a phase-separated blend involves the thermal excitation of both the electron and the hole to their respective transport energies. As a consequence, charge encounter is more affected by increased disorder than resplitting of the CT state, causing a recombination reduction factor as small as 10^{-3} for high disorder and high attempt-to-hop frequencies. Such conditions are reported for fullerene-based blends and are a possible reason for the highly suppressed recombination in some fullerene-containing bulk-heterojunction solar cells.

A. Theory

In the following, we briefly review free charge recombination through the formation and decay of CT states. The states and rates involved in this process are depicted in Fig. 1. A more detailed treatment, including the reformation of singlet states or the buildup of triplet population, is described in detail in Refs. [32,33], but the inclusion of these states does not change the general conclusions.

In the absence of generation, the kinetics of the excited-state population is determined by the following two differential equations [19]:

$$\frac{dn_{\text{CS}}}{dt} = -\beta_{\text{enc}}n_{\text{CS}}^2 + k_d n_{\text{CT}}, \quad (4a)$$

$$\frac{dn_{\text{CT}}}{dt} = \beta_{\text{enc}}n_{\text{CS}}^2 - (k_d + k_f)n_{\text{CT}}. \quad (4b)$$

We now consider the case of a dynamic equilibrium between the free charges and CT states, where dn_{CT}/dt is smaller than the rates of the processes that increase or decrease the CT-state population, as expressed by

$\beta_{\text{enc}}n_{\text{CS}}^2 \cong (k_d + k_f)n_{\text{CT}}$. In this limit, R can be related to the free carrier density, n_{CS} , via

$$R = k_f n_{\text{CT}} = \frac{k_f}{k_d + k_f} \beta_{\text{enc}} n_{\text{CS}}^2 = \gamma_{\text{CT}} \beta_{\text{enc}} n_{\text{CS}}^2 \equiv k_2 n_{\text{CS}}^2. \quad (5)$$

Here,

$$\gamma_{\text{CT}} = \frac{k_f}{k_d + k_f}. \quad (6)$$

is the recombination reduction factor due to resplitting of the CT state.

For $k_d \ll k_f$, $\gamma_{\text{CT}} \cong 1$ and $R = R_{\text{enc}} = \beta_{\text{enc}}n_{\text{CS}}^2$, meaning that every charge pair forming a CT state will recombine. We denote this as the *encounter-dominated* recombination regime. It is common to relate β_{enc} to the charge carrier mobility via

$$\beta_{\text{enc}} = \gamma_{\text{enc}} k_L, \quad (7)$$

where $\gamma_{\text{enc}} (\leq 1)$ is the reduction factor due to the confinement of opposite charges in their nanodomains in a BHJ system (also called the geometric reduction factor). As a consequence, k_2 and R depend linearly on the sum of the charge carrier mobilities. For disordered systems, the mobility is given by the product of the carrier-hopping frequency, ν_0 , and a term describing the distribution of the hopping sites in space and energy. For a regular lattice and fully equilibrated carriers, this term becomes proportional to $\exp[-(4/9)(\sigma_{\text{DOS}}/k_B T)^2]$, where σ_{DOS} is the width of the Gaussian disorder [34,35]. Therefore, in the encounter-dominated case, k_2 will be linear with respect to ν_0 and decrease rapidly with increasing σ_{DOS} , while not depending on the CT decay rate, k_f .

In the other limit, $k_d \gg k_f$ and ($\gamma_{\text{CT}} \ll 1$). We denote this as the *resplitting-dominated* recombination regime. In this case, $\gamma_{\text{CT}} \cong k_f/k_d$ and Eq. (5) becomes

$$k_2 = k_f \frac{\beta_{\text{enc}}}{k_d} = k_f \frac{\gamma_{\text{enc}} k_L}{k_d}. \quad (8)$$

Here, the most important parameter that determines the suppression of recombination is $\gamma_{\text{enc}} k_L/k_d$, which expresses the interplay between CT formation and resplitting. In the absence of energetic disorder, results of KMC simulations on a lattice with lattice parameter a can be approximated by [36]

$$k_d = B k_L \frac{3}{4\pi a^3} \exp\left(-\frac{E_{\text{CS}} - E_{\text{CT}}}{k_B T}\right), \quad (9)$$

where B is a prefactor that depends on the lattice and interface morphology. For charge separation in a homogeneous

medium, $B \cong 0.5$, while $B = 5 - 15$ is found to give the best fit to the efficiency of charge separation in a phase-separated morphology, as simulated by KMC (note that in the seminal paper by Braun, $B = 1$). Irrespective of these details, Eq. (9) in combination with Eq. (8) predicts that k_2 becomes independent of the carrier mobilities for efficient CT resplitting due to the cancelation of k_L , but that it is largely determined by the energy and site densities of the contributing states. Clearly, the situation becomes more difficult in the presence of disorder, where there is a distribution of energies for both CT states and free charges. This is the main topic of this work.

B. Kinetic Monte Carlo modeling

The KMC algorithm has been introduced in previous works [37–42]. Details can be found in Appendix A. In brief, we consider a cubic lattice with lattice parameter $a_{\text{NN}} = 1.8$ nm, on which charges can hop to a fixed number of neighboring sites. For the current simulations we use 26 neighbors, which corresponds to a $3 \times 3 \times 3$ cube around each site. Hopping rates are calculated from the Miller-Abrahams expression with an attempt-to-hop frequency, ν_0 , that has the physical meaning of the success rate of downward hops to a nearest-neighbor site. For upward hopping, the rate is reduced accordingly. Following previous reports in the literature [41,43,44], we consider the range $\nu_0 = 10^8 - 10^{12}$ s⁻¹, which is large enough to clearly identify the different recombination regimes that are the topic of this work.

A statistical Gaussian disorder of width $\sigma_{\text{DOS}} = 65, 90$, or 120 meV is used. These values are chosen because they correspond to a stepwise 10 times reduction of the steady-state mobility at $T = 300$ K, while representing the range of disorder values reported for carrier transport in BHJ OSCs. For charge transport and recombination in fully homogeneous media, an effective hopping medium is defined with electron- and hole-hopping parameters and energies that correspond to the donor HOMO and acceptor LUMO level, respectively. Hereby, each site can function as a donor and acceptor. An on-site barrier for an electron-hole encounter is implemented to introduce a driving force for charge transfer and to avoid direct exciton formation. For phase-separated systems, the morphology is implemented by assigning individual hopping sites to different material phases. Here, we use a simplified phase-separated morphology consisting of 7×7 columnar inclusions in a 10×10 columnar unit cell, where the column axis is in the direction of charge extraction. Electron transfer to the acceptor phase is driven by a LUMO-level offset, $\Delta E^{\text{LUMO}} = E_{\text{donor}}^{\text{LUMO}} - E_{\text{acceptor}}^{\text{LUMO}} = 600$ meV (and for holes by a respective HOMO offset of 400 meV), to ensure the absolute separation of hole-electron pairs on site, as well as referring to common LUMO energies of -3.5 and -4.1 eV and HOMO energies of -5.5 and -5.9 eV

for donor and acceptor, respectively. In recent work, this morphology was demonstrated to be sufficient to describe device current-voltage characteristics [44]. We consider random energetic disorder and the same width of the DOS at the interface and in the bulk. We acknowledge that this approximation oversimplifies the energetics in a real BHJ blend with crystallized donor and acceptor domains and an intermixed interface. The simulation of such a complex morphology is beyond the scope of our paper, which is to establish fundamental correlations between energetic disorder, carrier mobility, and NGR. With the same argument, we refrain from introducing charge or CT delocalization.

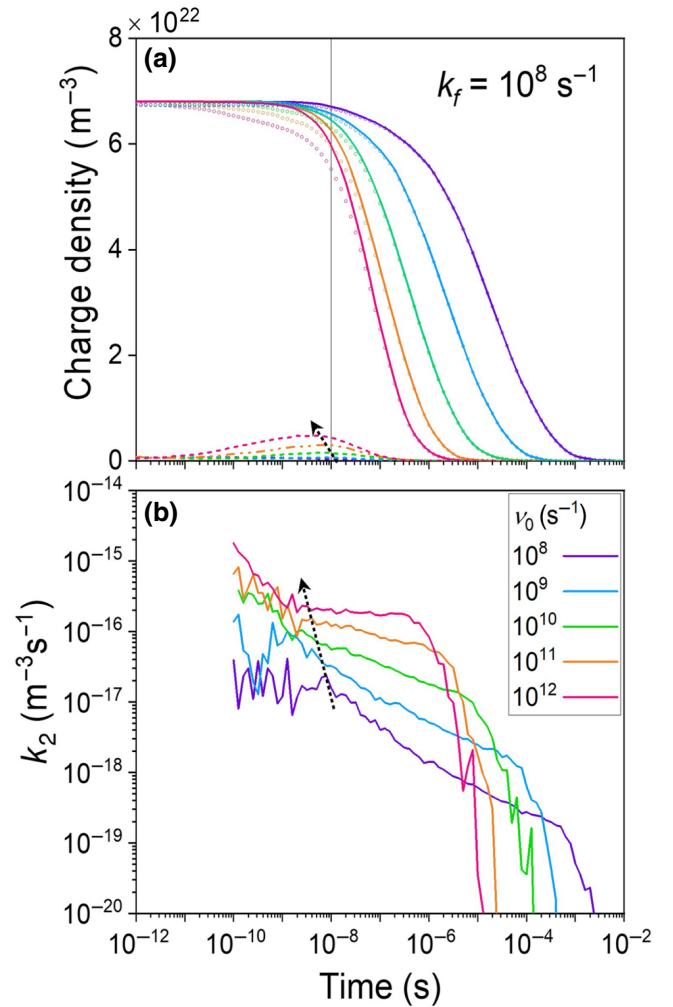


FIG. 2. KMC results of the dynamics of the total density of electron-hole pairs (solid lines), free electron-hole pairs (dotted lines), and CT states (dashed lines) for variable attempt-to-hop frequencies (ν_0) (a) and the corresponding second-order NGR coefficient (k_2) (b). Dotted arrows indicate the maximum CT population. Simulations are performed with the following parameters: $\sigma_{\text{DOS},e} = \sigma_{\text{DOS},h} = 90$ meV; $k_{\text{CT}} (k_f) = 1 \times 10^8$ s⁻¹; $T = 300$ K; intersite distance (a_{NN}) = 1.8 nm; $\nu_{0,e} = \nu_{0,h} = 1 \times 10^8, 10^9, 10^{10}, 10^{11},$ and 10^{12} s⁻¹ (purple to red).

II. RESULTS

Figure 2(a) shows an example of the temporal decay of n_{CT} , n_{CS} , and the total number of electron-hole pairs, $n = n_{CT} + n_{CS}$. The parameters are chosen to reproduce carrier densities and lifetimes, as typically reported for OSCs under steady-state illumination conditions [27,45–47]. Because we start with free charges distributed homogeneously on all donor and acceptor sites, the first step is the formation of an appreciable CT population due to free charge encounter, which for the phase-separated morphology requires the charges to meet at the donor-acceptor ($D-A$) heterojunction. Concurrently, the free carrier density decreases while the total number of charges remains rather constant during this process. This initial regime is followed by the decay of the carrier population via the decay of populated CT states to the ground state.

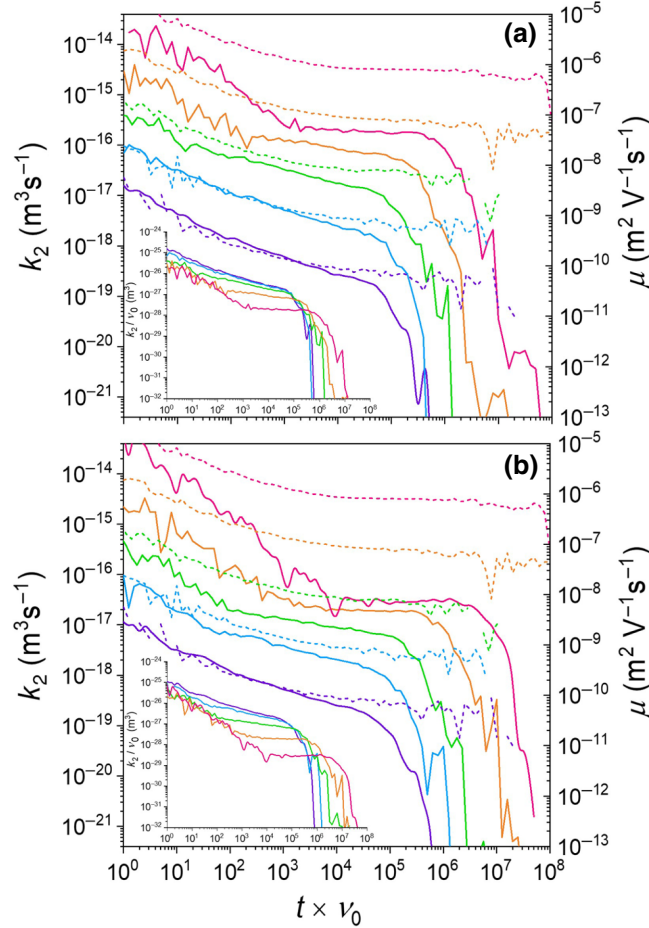


FIG. 3. Bimolecular recombination coefficient (solid lines) and charge carrier mobility (dashed lines) for variable attempt-to-hop frequencies at $k_f = 1 \times 10^8 \text{ s}^{-1}$ (a) and $1 \times 10^7 \text{ s}^{-1}$ (b), plotted as a function of $t\nu_0$. In both graphs, the two y axes are aligned according to the encounter-dominated case with $\gamma_{enc} = 0.4$. Insets show the corresponding k_2/ν_0 transients. KMC parameters are the same as those in Fig. 2.

Importantly, in this regime, $(dn_{CT}/dt) \ll (dn_{CS}/dt)$, meaning that dynamic equilibrium determines the CT-state population and the above considerations can be applied. As expected and shown before, increasing the hopping rate, ν_0 , speeds up recombination as charge encounter becomes more frequent, as seen by the continuous increase of the free charge NGR coefficient, k_2 , with ν_0 in Fig. 2(b). However, this increase becomes less pronounced at high ν_0 , indicating a transition to resplitting-dominated recombination.

A direct comparison of the carrier and CT kinetics for different ν_0 values is, however, difficult because the larger ν_0 is, the faster the equilibration of photogenerated charge carriers is in their respective DOS. A way out is to plot data as function of the reduced time $t\nu_0$, as documented for the time dependence of the corresponding mobility in Fig. 7 in Appendix B. Notably, when we additionally divide the mobility by ν_0 , the traces for different ν_0 values fall onto one line, despite different recombination properties for low and high hopping rates. This indicates that recombination does not concern predominately the faster carriers but rather affects the entire carrier population. Figure 3 compares $\mu(t\nu_0)$ to $k_2(t\nu_0)$ for $k_f = 10^8 \text{ s}^{-1}$ (a) and $k_f = 10^7 \text{ s}^{-1}$ (b). We are aware of the fact that a CT decay rate of 10^7 s^{-1} is at the very upper end of the reported values. As pointed out earlier, we deliberately chose a simple lattice model without charge or CT delocalization. This causes a fairly high CT binding energy of $E_{bind} = E_{CS} - E_{CT} = 228 \text{ meV}$ at $T = 300 \text{ K}$ for the chosen parameters and, concurrently, a small dissociation rate. However, all results and conclusions from this paper can be easily applied to the experimental situation by proper scaling of all rates. In Fig. 3, transient mobility data are aligned to the transient k_2 according to the encounter-limited case, where $k_2 = \gamma_{enc} k_L = \gamma_{enc} 2q\mu/\epsilon_0\epsilon_r$, thereby taking into account a slight suppression of encounter in the phase-separated morphology with $\gamma_{enc} = 0.4$.

For low ν_0 , k_2 is indeed dominated by charge encounter and is independent of k_f . On the other hand, the system enters the resplitting-dominated regime for a high enough ν_0 , where now k_2 becomes proportional to k_f but independent of ν_0 (and μ). In the most extreme case treated in Fig. 3, recombination is suppressed by 100 times. The transition from encounter- to resplitting-dominated recombination is more clearly seen in the insets, where we plot k_2/ν_0 as a function of $t\nu_0$, and where all curves with encounter-dominated recombination fall onto one line.

Figure 4 provides a more detailed look at the carrier dynamics for the case of $\sigma_{DOS} = 90 \text{ meV}$, $k_f = 10^8 \text{ s}^{-1}$ (see Fig. 8 in Appendix C for the same data but plotted as a function of time). As expected from the earlier observation that $\mu/\nu_0(t\nu_0)$ is independent of ν_0 , we observe very similar values and transients of the mean energy of the charges (a) and of the energy of moving charges (b) for different hopping rates when plotted as a

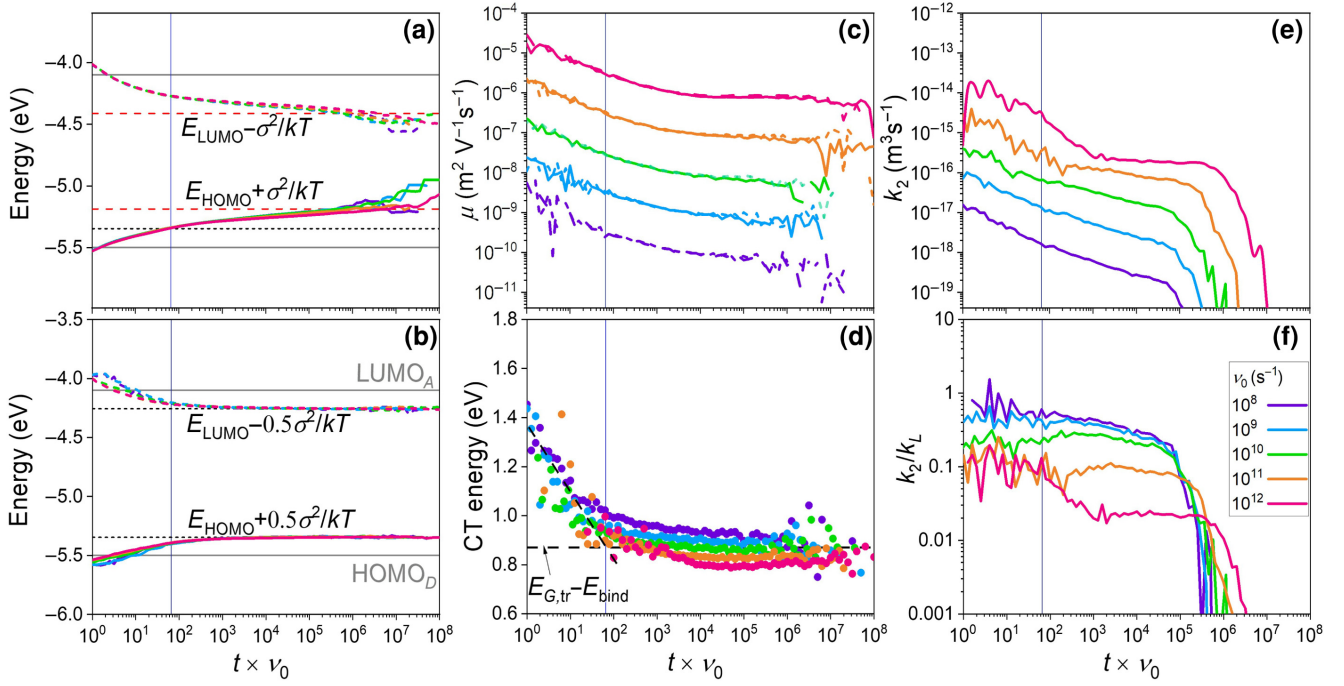


FIG. 4. Simulated transients of (a) mean energy of all charges, (b) mean energy of moving charges, (c) bipolar mobilities for holes (solid lines) and electrons (dashed lines), (d) energy of recombining CT states, (e) k_2 and (f) recombination reduction factor for variable attempt-to-hop frequencies plotted as a function of $t\nu_0$. KMC parameters are the same as those in Fig. 2. Blue vertical guideline marks the time when the mean energy crosses the transport energy $E_{tr} = E \mp \sigma_{DOS}^2/2k_B T$ (gray horizontal dashed guideline). Red horizontal guideline shows the equilibrium energy, $E_\infty = E \mp \sigma_{DOS}^2/k_B T$, where $-$ indicates electrons and $+$ indicates holes.

function of $t\nu_0$. As extensively discussed in the literature, the mean energy of the carriers continuously decreases and eventually approaches the energy of the equilibrated carriers, E_∞ , which for electrons (holes) is $\sigma_{DOS}^2/k_B T$ below (above) the center of the respective DOS. Because we start with free carriers distributed over the whole cell volume, the mean energy of the electrons (holes) is initially above (below) the center of the acceptor LUMO (donor HOMO). The blue vertical line marks the time when the mean energy crosses the effective transport energy ($E_{tr} = E_{LUMO} - \sigma_{DOS}^2/2k_B T$ for electrons and $E_{HOMO} + \sigma_{DOS}^2/2k_B T$ for holes). Once the carriers sink deeper into the DOS, their motion requires thermal excitation back to E_{tr} , as demonstrated by saturation of the energy of moving carriers in Fig. 4(b). Consequently, the carrier mobility reduces continuously even beyond this time [Fig. 4(c)]. In contrast, the mean energy of the recombining CT states shows a sudden transition to a nearly constant value once the carrier package crosses E_{tr} [see Fig. 4(d)]. Interestingly, this plateau is around an energy of

$$E = E_{G,tr} - E_{bind} = \left(E_{LUMO} - \frac{\sigma_{DOS,e}^2}{2k_B T} \right) - \left(E_{HOMO} + \frac{\sigma_{DOS,h}^2}{2k_B T} \right) - E_{bind},$$

which is the effective transport gap, $E_{G,tr}$, minus the CT binding energy. This suggests that once the carriers have moved deep into their respective DOS, CT states form predominately by the encounter of electrons and holes that are both traveling at their respective E_{tr} , while there is little contribution from equilibrated charges at E_∞ . A similar situation is encountered at lower and higher disorder values (Figs. 9 and 10 in Appendix C), where a transition to a nearly constant CT energy is seen when the carrier package crosses E_{tr} , although the transition is broader for high disorder. In all cases, data cluster around $E = E_{G,tr} - E_{bind}$ at long enough times after photogeneration (see Fig. 11 in Appendix D for the direct comparison of the three cases). It is suggested that CT formation in organic blends requires thermal excitation of at least one of the carriers up to the transport level [38,48]. Our data show that, in phase-separated blends, thermal excitation of both encountering carriers is involved in CT formation [30]. The situation is different in a fully intermixed system with otherwise identical parameters (Fig. 12 in Appendix D). Here, we observe a pronounced time dependence of the CT emission energy for all hopping rates, moving well below $E_{G,tr} - E_{bind}$ throughout the entire recombination process. This indicates that recombination between free and trapped carriers becomes the dominant channel for CT formation at longer times. Another important feature is

the slight downshift of the CT energy with increasing ν_0 . This shift occurs independent of whether recombination is encounter-dominated (every formed CT state recombines) or suppressed through CT resplitting. We propose that this process is mainly due to CT energy relaxation, although we cannot rule out contributions from the preferential resplitting of higher-energy CT states for large ν_0 . In both cases, the extent of the redshift is expected to increase with ν_0/k_f . This is well documented by the comparison of the CT transients for $k_f = 10^8 \text{ s}^{-1}$ and $k_f = 10^7 \text{ s}^{-1}$ in Fig. 12, where we observe the very same final energies for the same ν_0/k_f .

Figure 4(e) displays the time dependence of k_2 , while Fig. 4(f) shows the recombination reduction factor $\gamma = \gamma_{\text{geo}}\gamma_{\text{CT}}$. As discussed earlier, the initial free carrier loss is due to CT formation. Beyond this, the course of k_2 follows roughly the time dependence of μ , suggesting $k_2 \propto \mu$ (see

also Fig. 3). As a result, γ is nearly independent of time. While this is expected in the encounter-dominated case, where $\gamma = \gamma_{\text{enc}}$, our results suggest that γ_{CT} also exhibits only a weak (if any) time dependence in the resplitting-dominated regime, even when μ is time dependent. The effect is most pronounced for high disorder, where a continuous decrease of k_2 over time [Fig. 10(e)] contrasts a nearly time-independent reduction factor [Fig. 10(f)].

III. DISCUSSION

Before proposing a model to conclusively describe the simulation results, let us summarize the main findings. First, data show that a dynamic equilibrium exists between the mobile charges at E_{tr} and those situated deeper in the DOS for all conditions considered here, and this equilibrium is not severely disturbed by the formation and

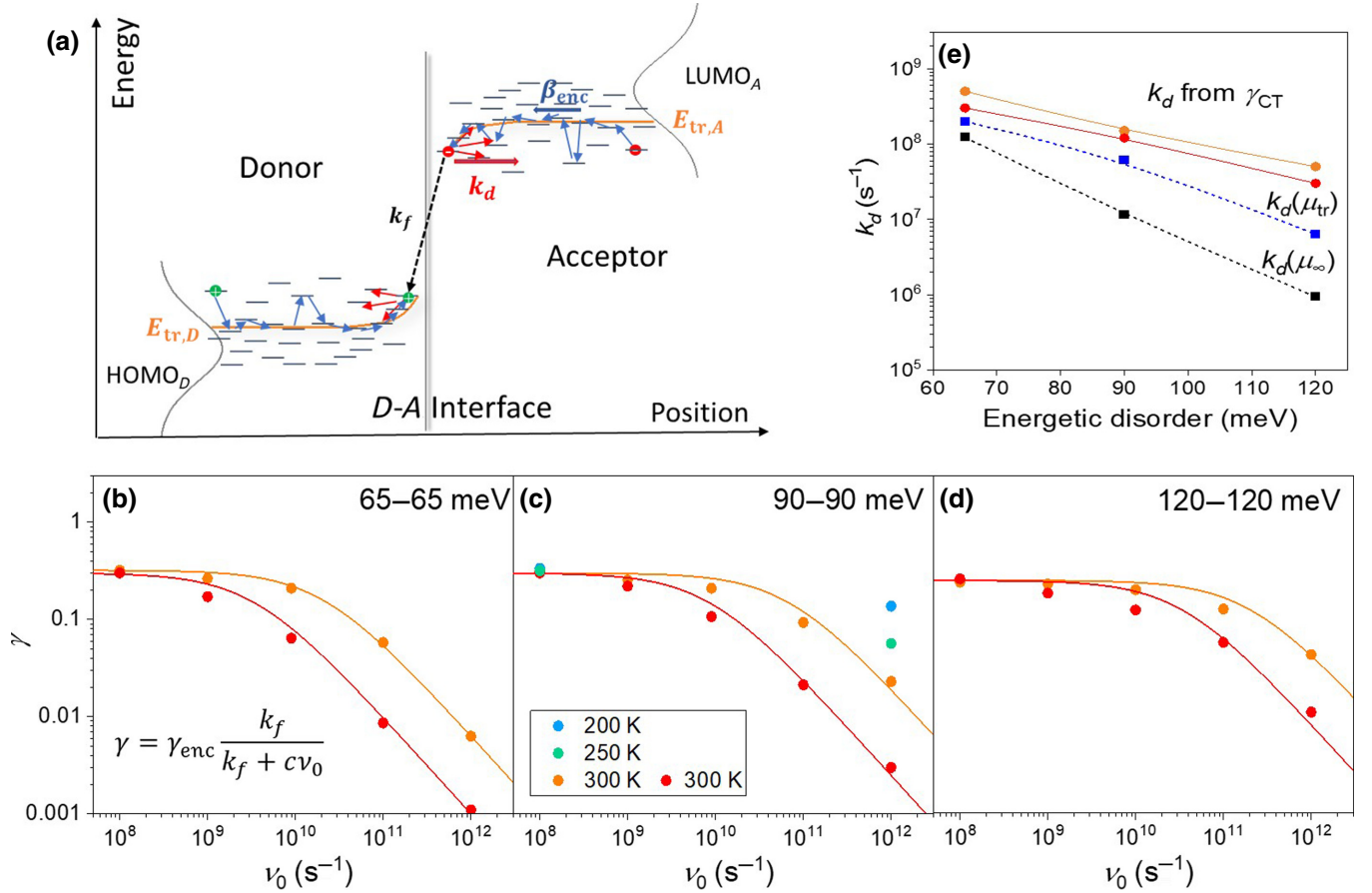


FIG. 5. (a) Scheme of CT formation, resplitting, and decay in a phase-separated disordered BHJ system. Charge encounter is determined by a time-dependent encounter rate, $\beta_{\text{enc}}(t) = \gamma_{\text{enc}}k_L[\mu(t)]$, involving the entire density of occupied states. In contrast, for long enough delay after photoexcitation, dissociation rate k_d is mainly determined by states around E_{tr} . (b)–(d) KMC results of the reduction factor γ of (nearly) equilibrated carriers for different hopping rates and disorders in phase-separated blends (taken at the times indicated in Fig. 13) for $k_f = 10^8 \text{ s}^{-1}$ (orange circles) and $k_f = 10^7 \text{ s}^{-1}$ (red circles). Solid lines show the best fit to data with Eq. (10). All simulations are performed at $T = 300 \text{ K}$, except for green ($T = 250 \text{ K}$) and blue ($T = 200 \text{ K}$) dots in (c). (e) k_d as a function of energetic disorder, as deduced from the fit of the reduction factor in (b)–(d) for $\nu_0 = 10^{11} \text{ s}^{-1}$ and $k_f = 10^8 \text{ s}^{-1}$ (see Table I for parameters). Also shown is the analytical prediction of k_d in the absence of disorder, according to Eq. (9), where μ is either the transient mobility when the carrier package crosses E_{tr} or after the carriers have equilibrated at E_{∞} (dotted lines).

TABLE I. γ_{enc} and c from the fit of the reduction factor in Figs. 5(b)–5(d) with Eq. (10) for different energetic disorder and CT decay time.

Energetic disorder (meV)	$k_f = 1 \times 10^8 \text{ s}^{-1}$		$k_f = 1 \times 10^7 \text{ s}^{-1}$	
	c	γ_{enc}	c	γ_{enc}
65–65	5×10^{-3}	0.32	3×10^{-3}	0.3
90–90	1.5×10^{-3}	0.3	1.2×10^{-3}	0.3
120–120	5×10^{-4}	0.25	3×10^{-4}	0.25

decay of the CT states. This is in accordance with the concept of the demarcation energy, E_D , as introduced by Refs. [20,29], where free charges in quasi-equilibrium with the main carrier distribution situated at E_D . As such, the rate at which charges encounter to form the CT state is determined by the mobility averaged over all carriers in the DOS. In accordance with this conclusion is the very weak effect of disorder and CT decay rate on the reduction factor in the encounter-dominated regime, as discussed in Appendix E and Fig. 13. Groves *et al.* reported a weak decrease of γ_{enc} by only 60% when increasing σ from 0 to 75 meV [17]. The observed range of values for γ_{enc} of 0.3–0.5 is fully consistent with the results of KMC with a disorder of 75 meV for a comparable domain size to that used here [18]. Second, data show that, once the carrier package has relaxed below E_{tr} , the mean energy of the recombining CT states is nearly time independent and close to the effective transport gap minus the CT binding energy. This is suggestive of a situation where CT formation is mainly by charges near E_{tr} . In our strict phase-separated blend, CT states are exclusively formed at the sharp D - A interface. Motion of the encountering charges in their respective phases towards this interface involves frequent trapping and re-excitation of these charges to E_{tr} , where it is more likely that charges meet at the interface when they are in a mobile state. In addition, an already existing electron (hole) at the D - A interface will tilt the DOS of the approaching countercharge, due to the mutual electrostatic interaction. As a consequence, hops to sites higher in the DOS will become more likely [34], an effect known as carrier heating by a strong electric field. In turn, the initial step of CT dissociation will mainly involve transport sites around the transport energy, leading to a very slow variation of k_d (and with that of γ_{CT}) with time, if any. This situation is depicted in Fig. 5(a).

Figure 13 in Appendix E plots the time dependence of γ for all cases studied here. Without phase separation, γ is equal to $\gamma_{\text{enc}} \cong 1$ in the encounter-dominated regime, but it becomes strongly time dependent once recombination becomes suppressed due to CT resplitting. This is explained by the continuous decrease of the CT energy, as documented in Fig. 12, suggesting that k_d is also time dependent. In contrast, for all phase-separated systems, there exists a plateau that extends over approximately 3

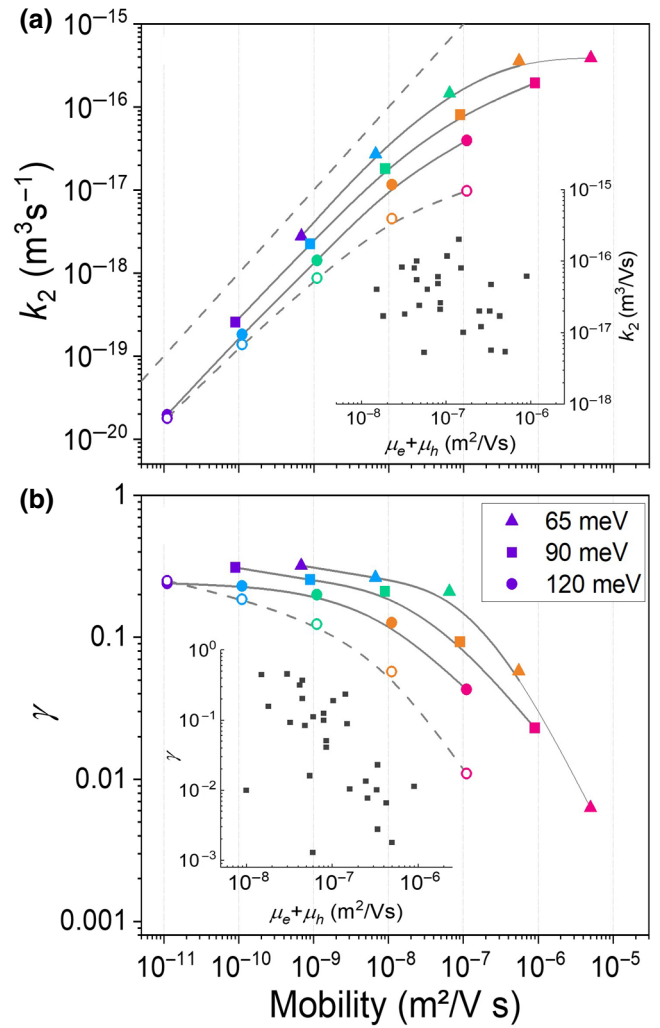


FIG. 6. Simulated k_2 as a function of μ_∞ for σ_{DOS} of 65 (triangles), 90 (squares), and 120 meV (circles) for (nearly) equilibrated charges taken at the times indicated in Fig. 13 (a) and the corresponding deduced reduction factor (b). Solid symbols indicate $k_f = 10^8 \text{ s}^{-1}$, while open circles show the results for $k_f = 10^7 \text{ s}^{-1}$ for the example of high energetic disorder. Dashed line is the prediction of the Langevin model; solid line guides the eye. Insets show experimental k_2 and γ data as a function of $\mu_e + \mu_h$ of bulk-heterojunction solar cells taken from Ref. [33] (gray dots).

orders in time (gray dashed line), even for the highly suppressed cases. For large disorder, this plateau is overlaid by a global decrease of γ with time, which is, however, far weaker than the decrease in μ over the considered time range.

Figures 5(b)–5(d) plot the reduction factor from these plateau regions versus the hopping rate. Regimes of encounter-dominated and resplitting-dominated recombination are clearly discernible. In the latter regime, increasing the disorder for a given hopping rate increases γ

(rendering recombination less suppressed) because CT dissociation slows down and becomes less competitive with CT dissociation decay. For the same reasons, a slower CT decay (smaller k_f) will decrease γ . To get a more quantitative picture, the simulation data are modeled by assuming that k_d is time independent and (for a given σ_{DOS}) strictly proportional to ν_0 , $k_d = c\nu_0$. Here, c is a dissociation prefactor, which is determined by details of the blend morphology and energetics but is independent of the kinetic parameters ν_0 and k_f . Accordingly,

$$\frac{k_2}{k_L} = \gamma = \gamma_{\text{enc}}\gamma_{\text{CT}} = \gamma_{\text{enc}} \frac{k_f}{k_f + k_d} = \gamma_{\text{enc}} \frac{k_f}{k_f + c\nu_0}, \quad (10)$$

with γ_{enc} and c being the only fitting parameters. The best fits are shown as solid lines in Figs. 5(b)–5(d), with the fitting parameters listed in Table I. Despite the simplicity of the model, the course of $\gamma(\nu_0)$ is well captured, with a very small dependence of the dissociation prefactor, c , on the CT decay rate. When σ_{DOS} increases from 65 to 120 meV, c (and with that k_d) decreases by circa 1 order of magnitude, while μ drops by a factor of 100, meaning that

the dissociation rate is less affected by disorder than the global mobility. This is in agreement with our model that charge encounter causes an athermal CT population, which is more prone to redissociation than a fully thermalized population.

Figure 5(e) plots k_d , as deduced from the fits in Fig. 5, for $\nu_0 = 10^{11} \text{ s}^{-1}$. Because of the presence of energetic disorder, an analytical model to describe the dependence of k_d on σ_{DOS} is unfortunately not available. Instead, we add to Fig. 5(e) the analytical predictions for k_d in the absence of disorder [Eq. (9)], where for μ we either insert the mobility at the time when the carrier package crosses E_{tr} (representative of the energy of carriers dissociating from the CT state) or after the carrier population is equilibrated at E_{∞} (describing the encounter of equilibrated carriers). Furthermore, $B = 10$, $a = 1.8 \text{ nm}$, and $E_{\text{bind}} = 228 \text{ meV}$. We find that $k_d(\mu_{\infty})$ displays a much stronger dependence on σ_{DOS} , lying 2 orders of magnitude below k_d from the recombination analysis at the largest disorder. In contrast, $k_d(\mu_{\text{tr}})$ captures quite well the σ_{DOS} dependence of k_d , although it underestimates its value for high disorder. This can be understood by the lowering of

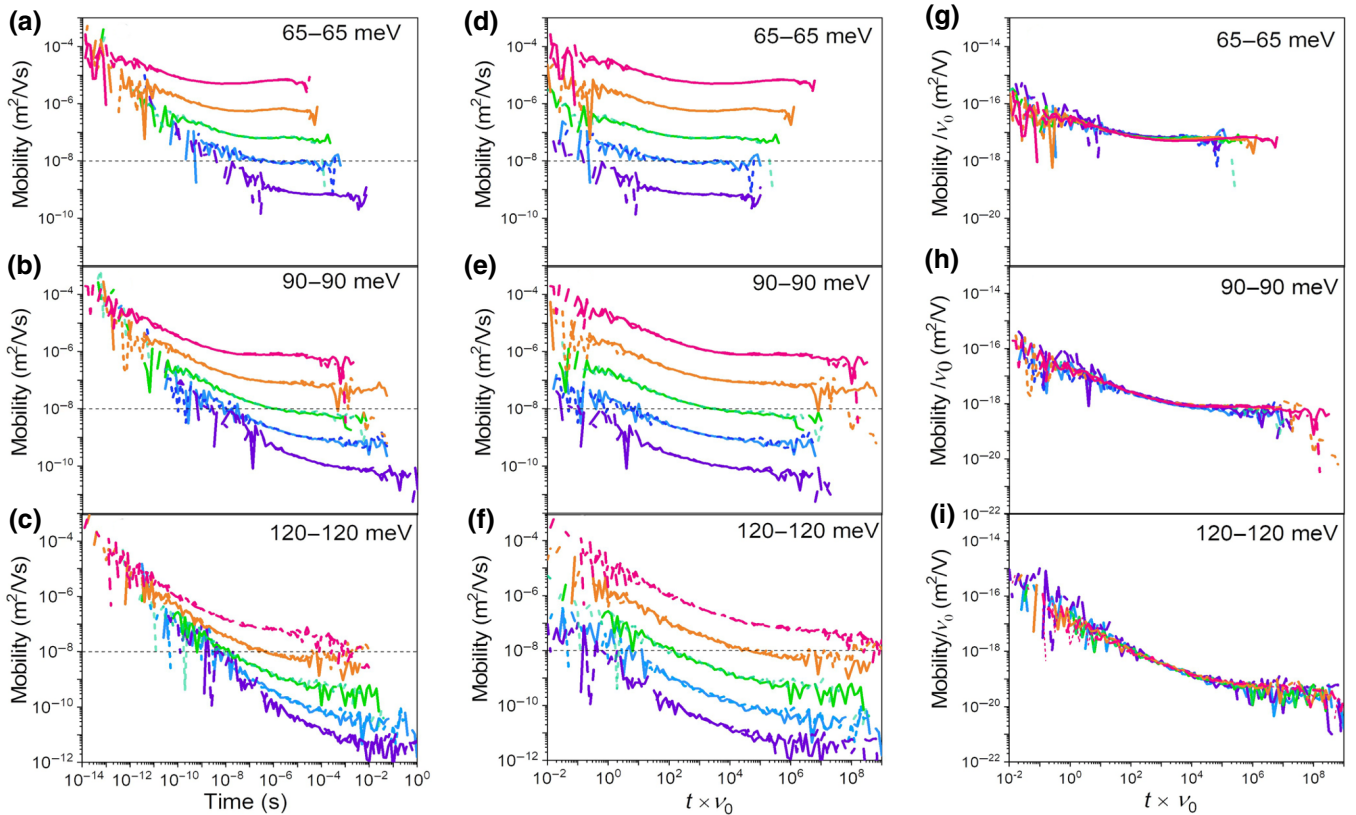


FIG. 7. Transient mobility as a function of time (a)–(c) and reduced time ($t\nu_0$) (d)–(f) for a phase-separated blend for variable energetic disorder and hopping frequencies under a voltage of 1 V. Universal mobility plot (g)–(i) with both mobility (μ/ν_0) and time ($t\nu_0$) modified by attempt-to-hop frequency ν_0 . Simulations are performed for $\sigma_{\text{DOS},e} = \sigma_{\text{DOS},h} = 65$ (a),(d),(g), 90 (b),(e),(h), and 120 meV (c),(f),(i); $T = 300 \text{ K}$; $a_{\text{NN}} = 1.8 \text{ nm}$; $k_{\text{CT}} (k_f) = 1 \times 10^8 \text{ s}^{-1}$; $\nu_{0,e} = \nu_{0,h} = 1 \times 10^8, 10^9, 10^{10}, 10^{11}, \text{ and } 10^{12} \text{ s}^{-1}$ (purple to red), respectively.

the effective dissociation barrier due to energetic disorder, which is well-documented in the literature and is not captured by Eq. (9) [49,50]. Nevertheless, the benefit of increased energetic disorder in providing a larger number of low-energy states for free carriers is overcompensated by a reduced mobility, resulting overall in a decrease of k_d .

To complement our study, we perform additional simulations at different temperatures with $\sigma_{\text{DOS}} = 90$ meV, $k_f = 10^8$ s $^{-1}$, and ν_0 set to either 10^8 (encounter dominated) or 10^{12} s $^{-1}$ (resplitting dominated), see Appendix F. The resulting transients of k_L , k_2 , and γ are shown in Fig. 14. Decreasing the temperature from 300 to 200 K slows down thermalization, as seen by more pronounced dispersive effects. Importantly, in the encounter-limited regime, k_2 decreases in the same way with temperature and time as μ , meaning that γ ($= \gamma_{\text{enc}}$ in the encounter-dominated case) is barely affected by temperature [Figs. 8(a) and 8(c)]. This confirms our interpretation that the rate at which CT states form is governed by the motion of carriers towards the heterojunction and that the final step of CT formation state is not the rate-limiting step. Figures 14(b) and 14(d) display the situation for the resplitting-dominated case. Here, the effect of temperature on k_2 is much weaker than that on μ , causing an about 10

times increase of γ from 300 to 200 K. This is the consequence of the need for thermal excitation to dissociate the CT state into free charges [Eq. (9)], meaning that CT dissociation competes less efficiently with CT decay at lower temperatures.

Our model has important consequences for the conditions to be met when aiming for strongly suppressed free carrier recombination despite a high carrier mobility. Figure 15 in Appendix G collects k_2 , μ , and γ for (nearly) equilibrated carriers. For a given disorder, increasing ν_0 (and with that μ) causes a transition from the encounter- to the resplitting-dominated regime. Above this transition, i.e., in the resplitting-dominated regime, a further increase of ν_0 (μ) leaves k_2 nearly unaffected [see also Fig. 6(a)]. High hopping rates are, therefore, indispensable when aiming for a favorable extraction-recombination balance, which is in full agreement with the prediction of the simple rate model in Sec. III. Reducing the energetic disorder, e.g., by removing impurities or improving the domain crystallinity, moves this transition to lower ν_0 . In the resplitting-dominated regime, a smaller σ increases k_2 but to a smaller extent than μ . This is the consequence of competition between the two processes that determine k_2 , namely, the increase of β_{enc} , which favors CT formation,

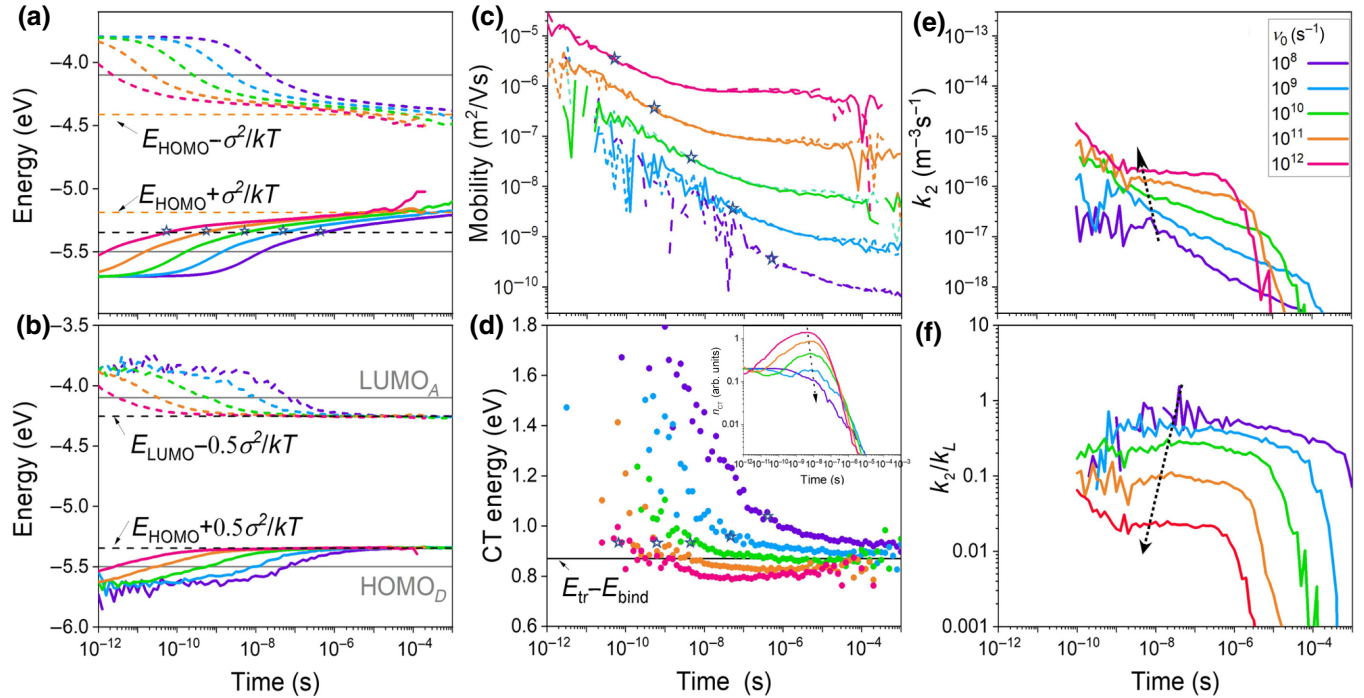


FIG. 8. Simulated transients for energetic disorder $\sigma_{\text{DOS},e} = \sigma_{\text{DOS},h} = 90$ meV of (a) mean energy of charges, (b) energy of moving charges, (c) bipolar mobilities for holes (solid lines) and electrons (dashed lines), (d) energy of recombining CT states (e) of k_2 and (f) of the reduction factor for variable attempt-to-hop frequencies plotted as a function of time (see Fig. 3 for the corresponding plot as a function of ν_0). KMC parameters are the same as those in Fig. 3(a). Star symbol marks the time when the mean energy crosses the effective transport energy, $E_{\text{tr}} = E \mp \sigma_{\text{DOS}}^2/2k_B T$ (gray horizontal dashed guideline), for different ν_0 , and orange horizontal guideline shows the equilibrium energy, $E_{\infty} = E \mp \sigma_{\text{DOS}}^2/k_B T$, where $-$ corresponds to electrons and $+$ to holes. $E_{G,\text{tr}} - E_{\text{bind}} = [E_{\text{LUMO}} - (\sigma_{\text{DOS},e}^2/2k_B T)] - [E_{\text{HOMO}} + (\sigma_{\text{DOS},h}^2/2k_B T)] - E_{\text{bind}}$. Arrow indicates maximum CT population.

and more efficient CT resplitting due to a larger k_d . Therefore, for a given value of ν_0 , the extraction-recombination balance benefits from lower disorder. A more complete picture (Fig. 6) arises when plotting k_2 and γ as a function of mobility, a combined function of the hopping rate and the energetic disorder,

$$\mu_\infty \propto \nu_0 \exp \left[-\frac{4}{9} \left(\frac{\sigma_{\text{DOS}}}{k_B T} \right)^2 \right].$$

For low mobility, k_2 is almost entirely determined by mobility, and does not depend explicitly on the energetic disorder. In contrast, mobility is not a decisive parameter for k_2 in the resplitting-dominated recombination regime. Instead, k_2 becomes a sole function of the morphology, CT and CS energetics, and CT-state decay properties. Our simulations, therefore, predict a large variation of k_2 for a given mobility in the resplitting-dominated regime. This is found experimentally, see the insets of Fig. 6. As expected, the scatter of the experimental values is larger than of the KMC data in Fig. 6, which is due to the fact that other parameters than considered in our simulations (interface morphology, CT delocalization), contribute to k_d and with that to k_2 . As a consequence, it should be possible to decrease the FOM, α , in Eq. (2) towards the Shockley

regime ($\alpha < 1$) by independently reducing k_2 and increasing μ through proper design of the molecular and blend structures.

Noticeably, for a given mobility, our simulations show that the larger σ_{DOS} is, the smaller k_2 is, and stronger CT resplitting will reduce recombination. This is again a direct consequence of the dependence of k_2 on k_d and β_{enc} , where increasing disorder slows down β_{enc} more strongly than k_d . In turn, if we consider k_2 for a given mobility, a large disorder combined with a high hopping rate is desirable. Soluble fullerenes, are known to exhibit considerable energetic disorder while also having large hopping rates [37,41,42,51,52]. For example, analysis of the transient carrier collection in the blend of [6,6]-phenyl-C71-butyric acid methyl ester (PC₇₁BM) with the donor polymer poly[2,3-bis(3-octyloxyphenyl)quinoxaline-5,8-diyl-alt-thiophene-2,5-diyl] (TQ1) through KMC yielded $\sigma_{\text{DOS},e} = 125$ meV and $\nu_e = 1.8 \times 10^{13} \text{ s}^{-1}$. Substituted fullerenes, such as PCBM, have fairly small aggregate sizes even in phase-separated blends [53], while they exhibit significant orientational and conformational disorder within these crystallites [54]. Combined with dynamic disorder due to electron-vibration coupling, values of σ as large as 100 meV are predicted for crystalline PCBM clusters [55]. On the other hand, the close distance and near-spherical shape of fullerene's

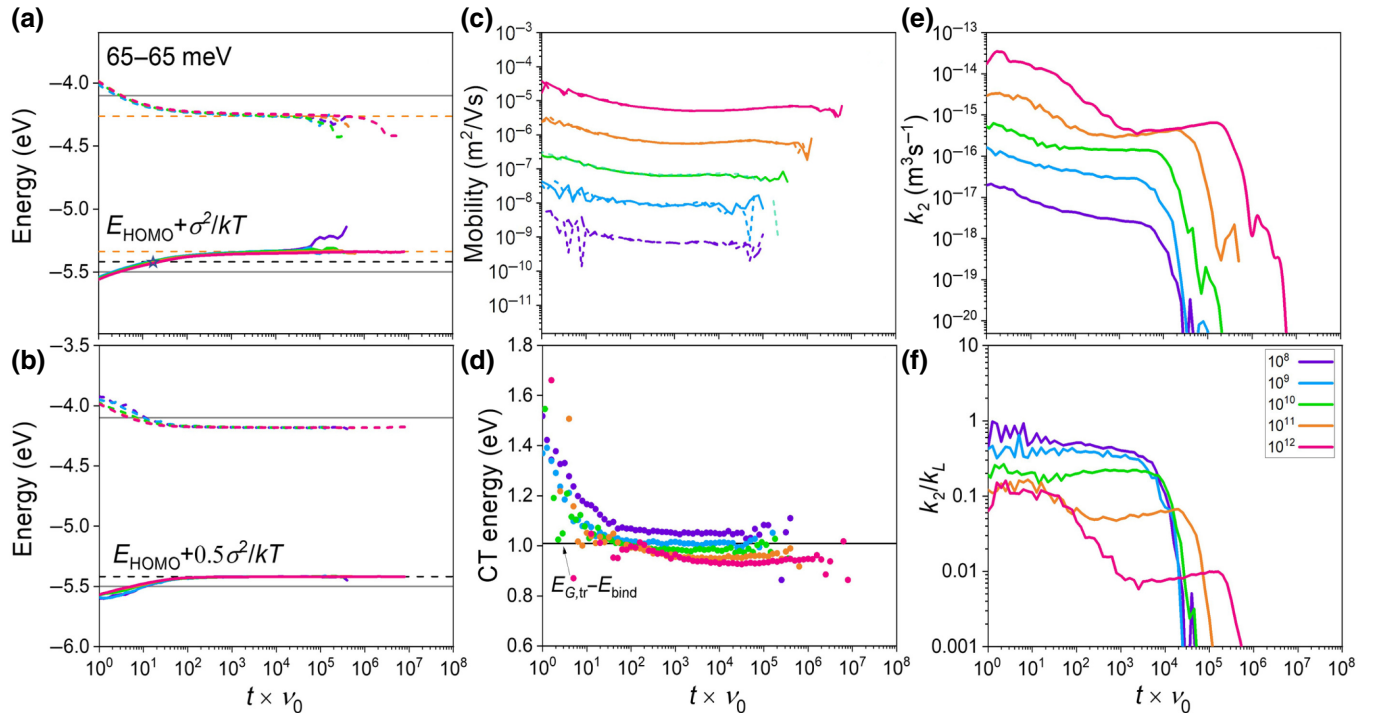


FIG. 9. Simulated transients for energetic disorder $\sigma_{\text{DOS},e} = \sigma_{\text{DOS},h} = 65$ meV of (a) mean energy of charges, (b) energy of moving charges, (c) bipolar mobilities for holes (solid lines) and electrons (dashed lines), (d) energy of recombining CT states (e) of k_2 and (f) of the reduction factor for variable attempt-to-hop frequencies plotted as a function of $t\nu_0$. KMC parameters as well as the meaning of all symbols and lines are the same as those in Fig. 3 except for the energetic disorder.

conjugated orbitals result in large electron coupling, which explains the overall high electron mobility [54,56]. Modern NFAs, as used in state-of-the-art OSCs, exhibit highly crystalline layers with energetic disorders of typically 50–70 meV [46,57–59]. Unfortunately, only a few studies concern the interplay between free carrier recombination and motion in NFA-based blends, [46,60–62] and even fewer include the measurement of energetic disorder [46,47,57,59]. These studies yield a fairly wide spread of mobilities and recombination coefficients, even for the same material combination, which may, in part, be related to details of the molecular structure (e.g., the polymer molecular weight [62,63]) or the layer morphology (e.g., interface properties [31,64]). Therefore, experimental studies on well-defined morphologies are urgently needed to disentangle the different processes that govern the mobility-recombination interplay in high-performance NFA-based systems.

IV. CONCLUSION

We employ kinetic Monte Carlo simulations to understand transient free carrier motion and recombination in energetically disordered phase-separated donor-acceptor blends. We find that the bimolecular recombination coefficient can be described by competition between the free charge encounter, CT-state resplitting, and CT decay, as summarized by $k_2(t) = [(k_f)/(k_f + cv_0)]\gamma_{\text{enc}}k_L(t)$. Here, c describes the proportionality between the CT dissociation rate and the attempt-to-hop frequency, v_0 , and depends only on the energetics and structure of the phase-separated system but not on the details of the free carrier distribution in the DOS. This is a direct consequence of that fact that the free charge encounter in the considered phase-separated disordered D - A blend forms an athermal excited CT-state distribution, the energy of which is independent of the mean energy of the free carriers once the carrier population has moved below the effective transport energy. Despite this, the formation of the CT state is strictly proportional to the mobility averaged over all carriers, as expressed by the Langevin encounter coefficient, k_L . For high enough v_0 , the recombination coefficient becomes nearly independent of the attempt-to-hop frequency and, for a given energetic disorder, of the value of mobility. As such, mobility is no longer a decisive parameter for the value of k_2 in the resplitting-dominated regime. This opens a wide range of options for optimizing the extraction-recombination balance. We also show that energetic disorder affects charge encounters more than CT dissociation. As a consequence, decreasing the disorder increases μ more than k_2 . On the other hand, for a given mobility, a larger disorder and, hence, a larger hopping rate is preferred when aiming for highly suppressed recombination. Our simulations suggest energetic disorder as an important parameter to be considered when aiming for a

detailed understanding of nongeminate recombination in solar cells based on disordered semiconductors.

ACKNOWLEDGMENTS

G.Z. and S.S. thank the Alexander von Humboldt Foundation for funding. S.S. and D.N. acknowledge funding from the Deutsche Forschungsgemeinschaft (DFG, German Research Foundation through the project Fabulous (Grants No. NE 410/20 and No. SH 1669/1-1). M.K. thanks the Carl Zeiss Foundation for financial support. We also thank Sebastian Wilken (Åbo Akademi University) as well as Oskar Sandberg and Ardan Armin (Swansea University) for their careful reading of the manuscript and for fruitful discussions.

APPENDIX A: DETAILS OF THE KMC SIMULATION

Charge transport is described as a hopping process based on Miller-Abrahams rates, in which hopping with rate v_{ij} from an initial state i with energy E_i to a final state j with energy E_j , separated by a distance r_{ij} , is given by

$$v_{ij} = \begin{cases} v'_0(r_{ij}) \exp\left(-\frac{\Delta E}{k_B T}\right), & \Delta E > 0, \\ v'_0(r_{ij}), & \Delta E \leq 0, \end{cases}$$

where v'_0 is the rate of downward hopping and $\Delta E = E_j - E_i \pm q\vec{r}_{ij} \cdot \vec{F} + \Delta E_C$, with \vec{F} as the external electric field, \vec{r}_{ij} as the vector connecting initial and final sites, and q as the positive elementary charge. The $+$ ($-$) sign refers to electron (hole) hopping. The term ΔE_C is the change in Coulomb energy, as calculated by explicit evaluation of the interaction of the moving charge with (a) all other charges in the simulated device and (b) their image charges, as well as of the interaction of the image charges of the moving particle with (c) the particle itself and (d) all other particles. To avoid divergences at zero separation, the Coulomb

TABLE II. Key parameters used in KMC simulations.

Parameter	Value
Box size (sites)	$30 \times 30 \times 56$
Intersite distance, a_{NN} (nm)	1.8
Energetic disorder, $\sigma_{\text{DOS},e} = \sigma_{\text{DOS},h}$ (meV)	65, 90, 120
Attempt-to-hop frequency, $v_{0,e} = v_{0,h}$ (s^{-1})	1×10^8 to 10^{12}
Rate of CT-state recombination, k_{CT} (s^{-1})	1×10^8 or 1×10^7
Rate of exciton recombination, k_{ex} (s^{-1})	1×10^9
Inverse localization length, α (m^{-1})	1.67×10^9
Temperature, T (K)	300
LUMO of donor, $E_{\text{donor}}^{\text{LUMO}}$ (eV)	3.5
HOMO of donor, $E_{\text{donor}}^{\text{HOMO}}$ (eV)	5.5
LUMO of acceptor, $E_{\text{acceptor}}^{\text{LUMO}}$ (eV)	4.1
HOMO of acceptor, $E_{\text{acceptor}}^{\text{HOMO}}$ (eV)	5.9

interaction between a pair of (unlike) charges with charges $E_C = -q/4\pi\epsilon_0\epsilon_r r_{eh}$, with $\epsilon_0\epsilon_r$ as the dielectric constant ($\epsilon_r = 3.6$) and r_{eh} as the electron-hole distance, is truncated at minus the approximate exciton binding energy, for which we choose $E_b^{\text{ex}} = 0.5$ eV. $k_B T$ is the thermal energy; the prefactor v'_0 is corrected for differences in the tunneling distance r_{ij} as

$$v'_0 = v_0 \exp[-2\alpha(r_{ij} - a_{\text{NN}})]$$

with α as the inverse localization radius.

The single-particle site energies, E_i , are drawn from a Gaussian distribution function:

$$f(E_i) = \frac{1}{\sqrt{2\pi\sigma^2}} \exp\left[-\frac{(E_i - E_0)^2}{2\sigma^2}\right]$$

with E_0 as the mean energy and σ as the broadening of the total DOS, N_0 . The HOMO and LUMO energies of a single site are assumed to be uncorrelated. For each initial site i , the number of possible final sites j is set to 26, reflecting a $3 \times 3 \times 3$ shell around the initial site.

Simulations are either performed in a homogeneous system, where each site can function as either donor or acceptor, or for a phase-separated morphology, as described in the text. Free holes and electrons are considered as initial carriers, homogeneously distributed on the donor and

acceptor sites. The positive and negative charge carriers can randomly form excitons or CT states before eventually leaving the system by recombination. Exciton diffusion by the Förster resonant energy transfer mechanism is explicitly accounted for. The transition rate is evaluated as

$$v_{ij}^F = v_{\text{ex}} \left(\frac{R_0}{r_{ij}}\right)^6$$

where R_0 is the Förster radius and k_{ex} is the radiative exciton decay rate. CT recombination with rate k_{CT} is allowed whenever a hole and an electron sit on neighboring sites. Since we are interested in intrinsic material properties, we use periodic boundary conditions in all directions (no contacts).

For recombination studies, the electric field is set to zero ($\vec{F} = 0$), which is equivalent to open-circuit conditions. The transient value of the bimolecular recombination factor, k_2 , is extracted from the simulations by

$$R = \frac{dn_{\text{CS}}(t)}{dt} = k_2(t)n_{\text{CS}}^2(t)$$

where $n_{\text{CS}} = n_{\text{total}} - (n_{\text{CT}} + n_{\text{ex}})$. Here, $n_{\text{CS}} = n_e = n_h$ is the density of charge-separated states; n_{total} is total density of electron-hole pairs; and n_{CT} and n_{ex} are the densities of CT states and excitons, respectively.

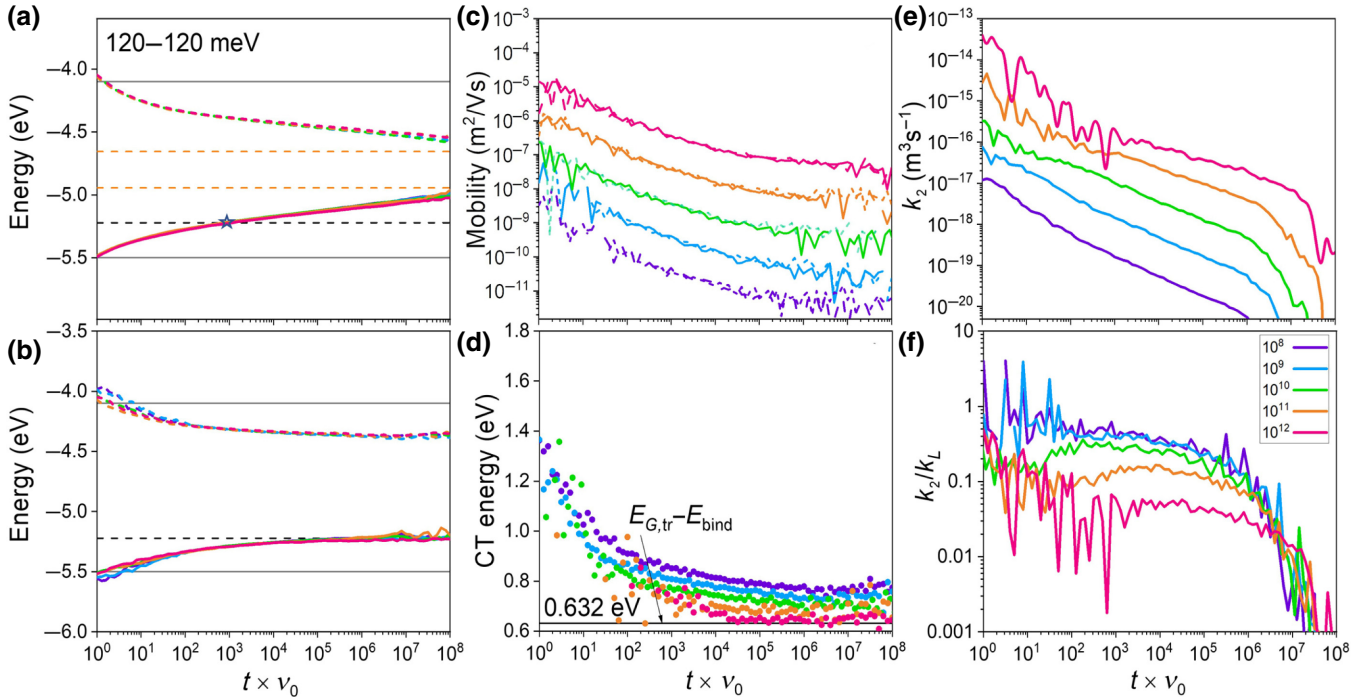


FIG. 10. Simulated transients for energetic disorder $\sigma_{\text{DOS},e} = \sigma_{\text{DOS},h} = 120$ meV of (a) mean energy of charges, (b) energy of moving charges, (c) bipolar mobilities for holes (solid lines) and electrons (dashed lines), (d) energy of recombining CT states (e) of k_2 and (f) of the reduction factor for variable attempt-to-hop frequencies plotted as a function of $t\nu_0$. KMC parameters as well as the meaning of all symbols and lines are the same as those in Fig. 3 except for the energetic disorder.

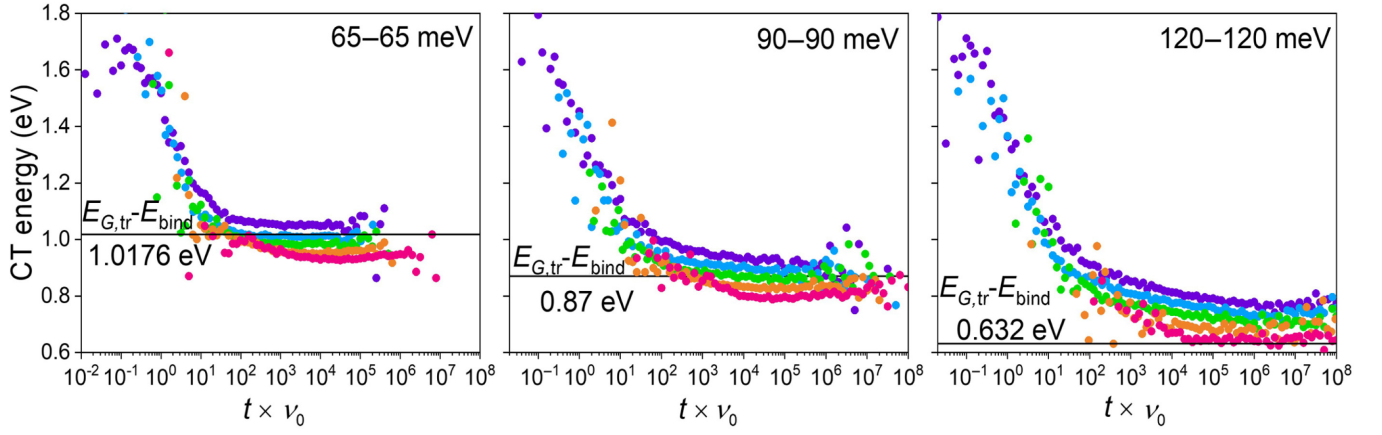


FIG. 11. Dynamics of the energy of recombining CT states as a function of reduced time for variable energetic disorder and hopping frequencies. $E_{G,\text{tr}} - E_{\text{bind}} = [E_{\text{LUMO}} - (\sigma_{\text{DOS},e}^2/2k_B T)] - [E_{\text{HOMO}} + (\sigma_{\text{DOS},h}^2/2k_B T)] - E_{\text{bind}}$. Except for energetic disorder, KMC parameters are the same as those in Fig. 2.

For the mobility calculations, a finite but low electric field of 1×10^7 V/m is used, and all other parameters are the same as those in corresponding recombination calculations (Table II).

APPENDIX B: TIME-DEPENDENT MOBILITY

Figure 7 shows transient mobilities, calculated with the same parameters as those used in the recombination simulations, but with an electric field of 1×10^7 V. Importantly, when the mobility and time are corrected for the hopping frequency, all transients merge for a given disorder.

APPENDIX C: TIME-DEPENDENT CARRIER EQUILIBRATION, MOTION, AND RECOMBINATION

Figure 8 shows the dependence of the characteristic carrier and CT properties with time after photoexcitation for

an energetic disorder of 90 meV and for different hopping rates, ν_0 . As expected from mobility data in Fig. 7, increasing ν_0 causes a total shift of the mean carrier energy [Fig. 7(a)] and of the energy of moving charges [Fig. 7(b)] as a function of lgt , without altering the shape of the transients. The same is (almost) true for the energy of the recombining CT state in Fig. 7(d). Stars in Figs. 8(a), 8(c), and 8(d) mark the time where the mean carrier energy crosses the transport energy, which is the time where the CT energy transitions to a constant value. In contrast to mobility data, the hopping rate has a pronounced effect on the recombination properties [Figs. 8(e) and 8(f)]. This is because of the transition between the encounter- and the resplitting-dominated regimes.

The transients of the same properties are plotted as a function of reduced time for disorders of 65 meV (Fig. 9) and 120 meV (Fig. 10). The huge effect of disorder on the time-dependence relaxation properties is clearly

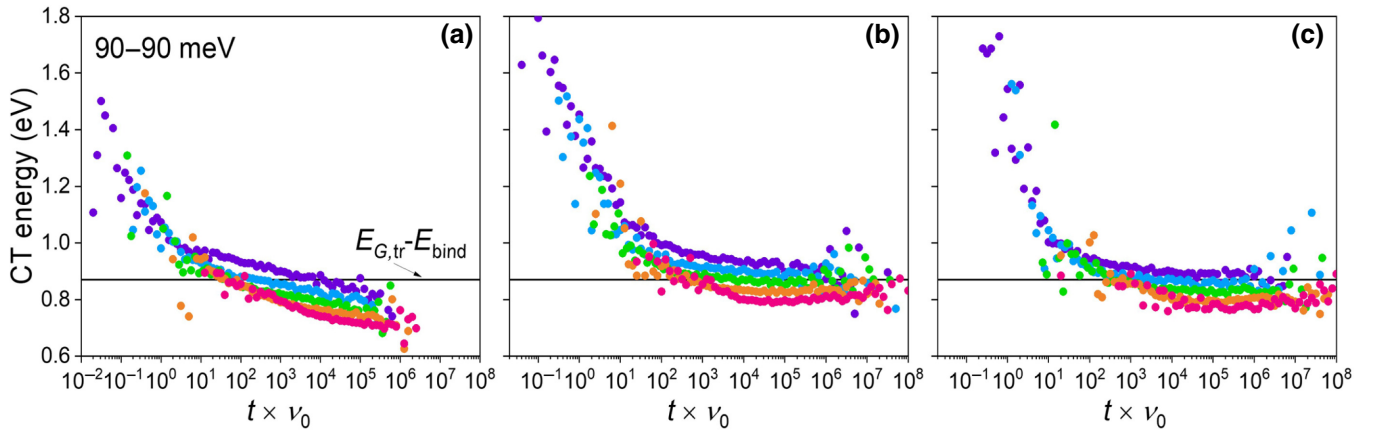


FIG. 12. Dynamics of the energy of recombining CT states as a function of reduced time for variable energetic disorder and hopping frequencies for a homogenous blend (a) and a phase-separated blend with $k_f = 1 \times 10^8$ s $^{-1}$ (b) and $k_f = 1 \times 10^7$ s $^{-1}$ (c).

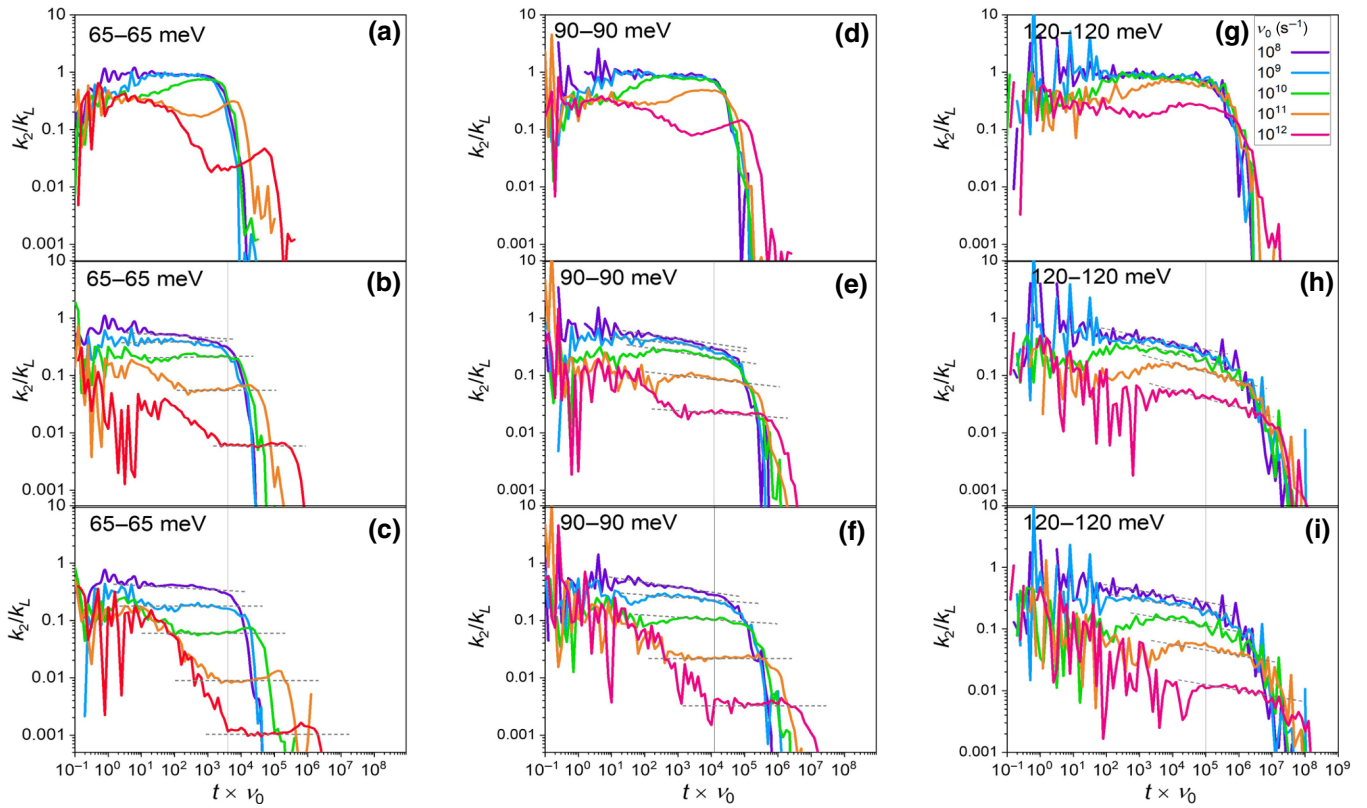


FIG. 13. Reduction factor $\gamma = k_2/k_L$ as a function of reduced time for either a homogeneous blend with $k_f = 1 \times 10^8 \text{ s}^{-1}$ (a),(d),(g), or a phase-separated blend with $k_f = 1 \times 10^8 \text{ s}^{-1}$ (b),(e),(h), or $k_f = 1 \times 10^7 \text{ s}^{-1}$ (c),(f),(i). Gray dashed lines highlight regions of (nearly) constant γ , from which data in Figs. 5 and 6 are deduced at the times marked by solid vertical lines.

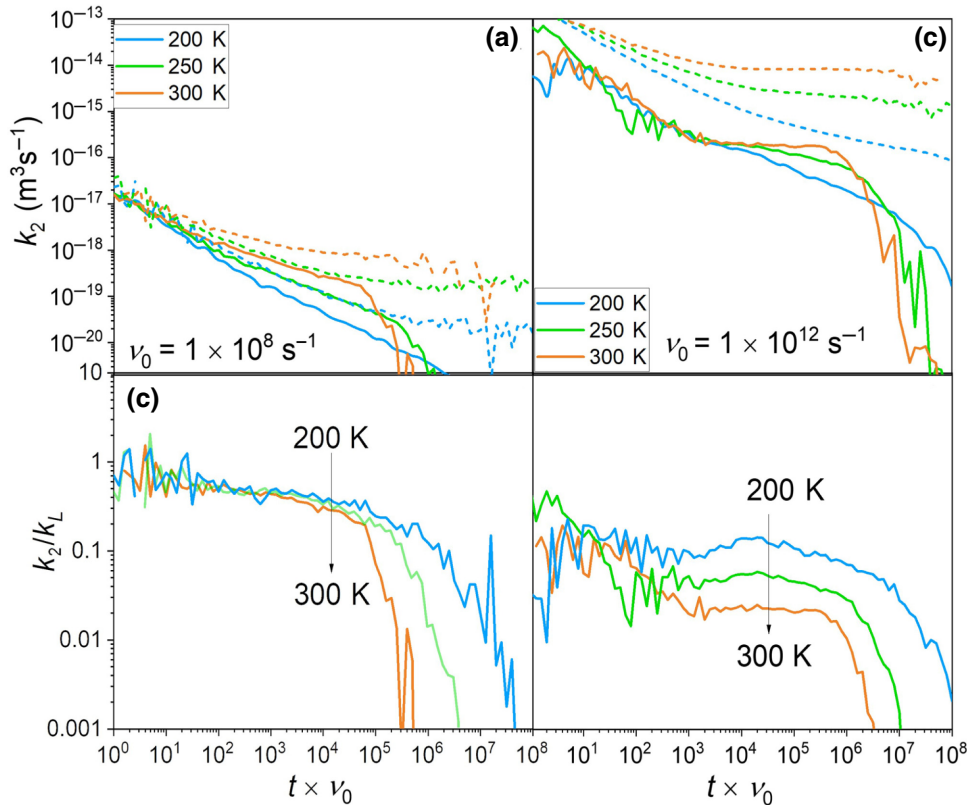


FIG. 14. Simulated transients of k_L (dashed lines) and k_2 (solid lines) (a),(b) and reduction factor γ (c),(d) as a function of reduced time for $\nu_0 = 10^8 \text{ s}^{-1}$ (a),(c) and $\nu_0 = 10^{12} \text{ s}^{-1}$ (b),(d) and different temperatures. $\sigma_{\text{DOS}} = 90 \text{ meV}$ and $k_f = 10^8 \text{ s}^{-1}$ in all cases.

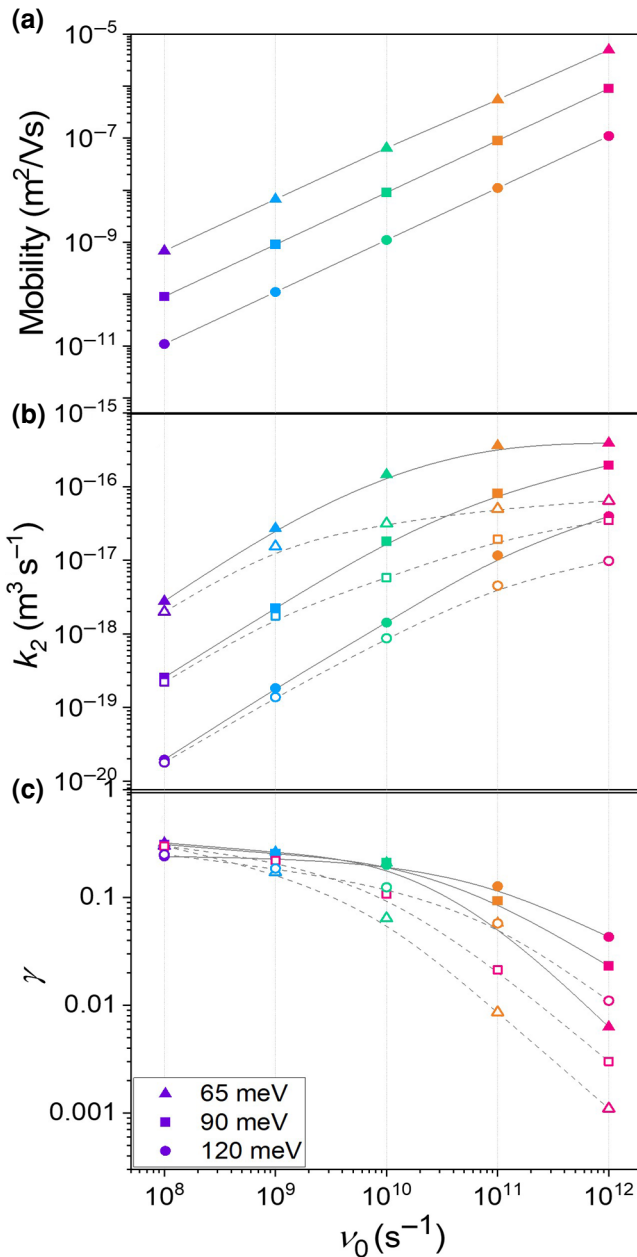


FIG. 15. Simulated values of mobility (a), k_2 (b), and reduction factor γ (c) for (nearly) equilibrated carriers, plotted as a function of hopping frequency for different energetic disorders, $\sigma_{\text{DOS}} = 65, 90, \text{ and } 120 \text{ meV}$, with $k_f = 10^8 \text{ s}^{-1}$ (solid lines) and $k_f = 10^7 \text{ s}^{-1}$ (dashed lines).

seen. Most importantly, while μ and k_2 exhibit a strong dependence on time for the high-disorder case, the reduction factor remains rather constant, irrespective of whether recombination is dominated by encounter or resplitting.

APPENDIX D: TIME DEPENDENCE OF THE RECOMBINING CT ENERGY

Figures 11 and 12 display the results of exemplary KMC simulations of the energy of the recombining CT state for

different conditions. Except for the case of a homogenous blend, the CT energy displays a transition from a steeply decaying time dependence to a constant value, which assembles around the effective transport energy minus the CT binding energy.

APPENDIX E: REDUCTION FACTOR

Figure 13 summarizes the transients of the reduction factor, $\gamma = k_2/k_L$, for all parameter sets treated in this work. The initial time range is dominated by the formation of the CT state by free carrier encounter. After this initial period, γ is nearly independent of time for all phase-separated blends, see the dashed lines. Notably, for small ν_0 (encounter-limited regime), disorder has little effect on γ , which varies only slightly between 0.3 and 0.5. For the homogenous blend, γ increases to one in the encounter-limited regime, meaning that $k_2 = k_L$. The resplitting-dominated regime of the homogeneous blend is determined by a significant time dependence of γ , where γ first decreases (CT formation) and then increases again. We assign the latter process to the progressive relaxation of the CT-state energy, rendering CT splitting more and more difficult.

APPENDIX F: REDUCTION FACTOR

Figure 14 shows simulated transients of k_2 , k_L , and $\gamma = k_2/k_L$ for three different temperatures. For slow hopping, $\nu_0 = 10^8 \text{ s}^{-1}$, decreasing the temperature reduces k_2 and k_L by the same amount for all times, rendering γ independent of temperature and time. This shows that the encounter rate is a simple function of the carrier mobility. The situation is different for slow hopping, $\nu_0 = 10^{12} \text{ s}^{-1}$, where a decreasing temperature reduces k_L significantly more than k_2 . As a consequence, recombination is more reduced at higher temperatures.

APPENDIX G: μ , k_2 , AND γ AS A FUNCTION OF HOPPING RATE

Shown in Fig. 15 is the dependence of μ , k_2 , and γ on hopping rate for three different disorders for nearly equilibrated charges. For a given hopping rate, increasing the disorder has little effect on γ in the encounter-dominated regime but increases γ in the resplitting-dominated regime. This is because a higher disorder slows down CT resplitting and, therefore, renders CT recombination more likely. Despite this, a larger σ will (in total) reduce k_2 because of slower charge encounter.

[1] C. Li, J. Zhou, J. Song, J. Xu, H. Zhang, X. Zhang, J. Guo, L. Zhu, D. Wei, G. Han, J. Min, Y. Zhang, Z. Xie, Y. Yi, H. Yan, F. Gao, F. Liu, and Y. Sun, Non-fullerene acceptors with branched side chains and improved molecular packing

- to exceed 18% efficiency in organic solar cells, *Nat. Energy* **6**, 605 (2021).
- [2] Q. Liu, Y. Jiang, K. Jin, J. Qin, J. Xu, W. Li, J. Xiong, J. Liu, Z. Xiao, K. Sun, S. Yang, X. Zhang, and L. Ding, 18% efficiency organic solar cells, *Sci. Bull.* **65**, 272 (2020).
- [3] F. Liu, L. Zhou, W. Liu, Z. Zhou, Q. Yue, W. Zheng, R. Sun, W. Liu, S. Xu, H. Fan, L. Feng, Y. Yi, W. Zhang, and X. Zhu, Organic solar cells with 18% efficiency enabled by an alloy acceptor: A two-in-one strategy, *Adv. Mater.* **33**, 2100830 (2021).
- [4] Y. Cui, H. Yao, J. Zhang, K. Xian, T. Zhang, L. Hong, Y. Wang, Y. Xu, K. Ma, C. An, C. He, Z. Wei, F. Gao, and J. Hou, Single-junction organic photovoltaic cells with approaching 18% efficiency, *Adv. Mater.* **32**, 1908205 (2020).
- [5] M. Zhang, L. Zhu, G. Zhou, T. Hao, C. Qiu, Z. Zhao, Q. Hu, B. W. Larson, H. Zhu, Z. Ma, Z. Tang, W. Feng, Y. Zhang, T. P. Russell, and F. Liu, Single-layered organic photovoltaics with double cascading charge transport pathways: 18% efficiencies, *Nat. Commun.* **12**, 1 (2021).
- [6] A. Karki, A. J. Gillett, R. H. Friend, and T. Q. Nguyen, The path to 20% power conversion efficiencies in non-fullerene acceptor organic solar cells, *Adv. Energy Mater.* **11**, 1 (2021).
- [7] D. Neher, J. Kniepert, A. Elimelech, and L. J. A. Koster, A new figure of merit for organic solar cells with transport-limited photocurrents, *Sci. Rep.* **6**, 24861 (2016).
- [8] S. Wilken, D. Scheunemann, S. Dahlström, M. Nyman, J. Parisi, and R. Österbacka, How to reduce charge recombination in organic solar cells: There are still lessons to learn from P3HT:PCBM, *Adv. Electron. Mater.* **7**, 2001056 (2021).
- [9] N. Gasparini, M. Salvador, T. Heumueller, M. Richter, A. Classen, S. Shrestha, G. J. Matt, S. Holliday, S. Strohm, H. J. Egelhaaf, A. Wadsworth, D. Baran, I. McCulloch, and C. J. Brabec, Polymer:Nonfullerene bulk heterojunction solar cells with exceptionally low recombination rates, *Adv. Energy Mater.* **7**, 1701561 (2017).
- [10] A. Armin, Z. Chen, Y. Jin, K. Zhang, F. Huang, and S. Shoaee, A shockley-type polymer: Fullerene solar cell, *Adv. Energy Mater.* **8**, 1701450 (2018).
- [11] A. Armin, J. Subbiah, M. Stolterfoht, S. Shoaee, Z. Xiao, S. Lu, D. J. Jones, and P. Meredith, Reduced recombination in high efficiency molecular nematic liquid crystalline: Fullerene solar cells, *Adv. Energy Mater.* **6**, 1600939 (2016).
- [12] K. N. Schwarz, P. B. Geraghty, V. D. Mitchell, S.-U.-Z. Khan, O. J. Sandberg, N. Zarrabi, B. Kudisch, J. Subbiah, T. A. Smith, B. P. Rand, A. Armin, G. D. Scholes, D. J. Jones, and K. P. Ghiggino, Reduced recombination and capacitor-like charge buildup in an organic heterojunction, *J. Am. Chem. Soc.* **142**, 2562 (2020).
- [13] W. Zhu, *et al.*, Crystallography, morphology, electronic structure, and transport in non-fullerene/non-indacenodithienothiophene polymer:Y6 solar cells, *J. Am. Chem. Soc.* **142**, 14532 (2020).
- [14] S. Roland, M. Schubert, B. A. Collins, J. Kurpiers, Z. Chen, A. Facchetti, H. Ade, and D. Neher, Fullerene-free polymer solar cells with highly reduced bimolecular recombination and field-independent charge carrier generation, *J. Phys. Chem. Lett.* **5**, 2815 (2014).
- [15] A. Pivrikas, G. Juška, A. J. Mozer, M. Scharber, K. Arlauskas, N. S. Sariciftci, H. Stubb, and R. Österbacka, Bimolecular Recombination Coefficient as a Sensitive Testing Parameter for low-Mobility Solar-Cell Materials, *Phys. Rev. Lett.* **94**, 176806 (2005).
- [16] L. J. A. Koster, V. D. Mihailetschi, and P. W. M. Blom, Bimolecular recombination in polymer/fullerene bulk heterojunction solar cells, *Appl. Phys. Lett.* **88**, 1 (2006).
- [17] C. Groves and N. C. Greenham, Bimolecular recombination in polymer electronic devices, *Phys. Rev. B - Condens. Matter Mater. Phys.* **78**, 1 (2008).
- [18] M. C. Heiber, C. Baumbach, V. Dyakonov, and C. Deibel, Encounter-limited Charge-Carrier Recombination in Phase-Separated Organic Semiconductor Blends, *Phys. Rev. Lett.* **114**, 1 (2015).
- [19] T. M. Burke, S. Sweetnam, K. Vandewal, and M. D. McGehee, Beyond langevin recombination: How equilibrium between free carriers and charge transfer states determines the open-circuit voltage of organic solar cells, *Adv. Energy Mater.* **5**, 1500123 (2015).
- [20] J. Orenstein and M. A. Kastner, Thermalization and recombination in amorphous semiconductors, *Solid State Commun.* **40**, 85 (1981).
- [21] J. Nelson, Diffusion-limited recombination in polymer-fullerene blends and its influence on photocurrent collection, *Phys. Rev. B* **67**, 155209 (2003).
- [22] T. M. Clarke, F. C. Jamieson, and J. R. Durrant, Transient absorption studies of bimolecular recombination dynamics in polythiophene/fullerene blend films, *J. Phys. Chem. C* **113**, 20934 (2009).
- [23] I. A. Howard, F. Etzold, F. Laquai, and M. Kemerink, Nonequilibrium charge dynamics in organic solar cells, *Adv. Energy Mater.* **4**, 1301743 (2014).
- [24] A. Hofacker, J. O. Oelerich, A. V. Nenashev, F. Gebhard, and S. D. Baranovskii, Theory to carrier recombination in organic disordered semiconductors, *J. Appl. Phys.* **115**, 1 (2014).
- [25] J. Kurpiers and D. Neher, Dispersive non-geminate recombination in an amorphous polymer:Fullerene blend, *Sci. Rep.* **6**, 26832 (2016).
- [26] A. Hofacker and D. Neher, Dispersive and steady-state recombination in organic disordered semiconductors, *Phys. Rev. B* **96**, 245204 (2017).
- [27] S. Roland, J. Kniepert, J. A. Love, V. Negi, F. Liu, P. Bobbert, A. Melianas, M. Kemerink, A. Hofacker, and D. Neher, Equilibrated charge carrier populations govern steady-state nongeminate recombination in disordered organic solar cells, *J. Phys. Chem. Lett.* **10**, 1374 (2019).
- [28] B. Xiao, P. Calado, R. C. I. MacKenzie, T. Kirchartz, J. Yan, and J. Nelson, Relationship Between Fill Factor and Light Intensity in Solar Cells Based on Organic Disordered Semiconductors: The Role of Tail States, *Phys. Rev. Appl.* **14**, 1 (2020).
- [29] J. Orenstein and M. Kastner, Photocurrent Transient Spectroscopy: Measurement of the Density of Localized States in a-As₂Se₃, *Phys. Rev. Lett.* **46**, 1421 (1981).
- [30] D. Rauh, C. Deibel, and V. Dyakonov, Charge density dependent nongeminate recombination in organic bulk heterojunction solar cells, *Adv. Funct. Mater.* **22**, 3371 (2012).

- [31] V. Coropceanu, J. L. Brédas, and S. Mehraeen, Impact of active layer morphology on bimolecular recombination dynamics in organic solar cells, *J. Phys. Chem. C* **121**, 24954 (2017).
- [32] O. J. Sandberg and A. Armin, Energetics and kinetics requirements for organic solar cells to break the 20% power conversion efficiency barrier, *J. Phys. Chem. C* **125**, 15590 (2021).
- [33] S. Shoaee, A. Armin, M. Stolterfoht, S. M. Hosseini, J. Kurpiers, and D. Neher, Decoding charge recombination through charge generation in organic solar cells, *Sol. RRL* **3**, 1900184 (2019).
- [34] H. Bässler, Charge transport in disordered organic photoconductors a monte carlo simulation study, *Phys. Status Solidi* **175**, 15 (1993).
- [35] J. Cottaar, L. J. A. Koster, R. Coehoorn, and P. A. Bobbert, Scaling Theory for Percolative Charge Transport in Disordered Molecular Semiconductors, *Phys. Rev. Lett.* **107**, 136601 (2011).
- [36] M. Wojcik, A. Nowak, and K. Seki, Geminate electron-hole recombination in organic photovoltaic cells. A semi-empirical theory, *J. Chem. Phys.* **146**, 54101 (2017).
- [37] A. Melianas, V. Pranculis, Y. Xia, N. Felekidis, O. Inganäs, V. Gulbinas, and M. Kemerink, Photogenerated carrier mobility significantly exceeds injected carrier mobility in organic solar cells, *Adv. Energy Mater.* **7**, 1602143 (2017).
- [38] A. Melianas, N. Felekidis, Y. Puttison, S. C. J. Meskers, O. Inganäs, W. M. Chen, and M. Kemerink, Nonequilibrium site distribution governs charge-transfer electroluminescence at disordered organic heterointerfaces, *Proc. Natl. Acad. Sci.* **116**, 23416 (2019).
- [39] G. Zuo, H. Abdalla, and M. Kemerink, Impact of doping on the density of states and the mobility in organic semiconductors, *Phys. Rev. B* **93**, 235203 (2016).
- [40] G. Zuo, Z. Li, O. Andersson, H. Abdalla, E. Wang, and M. Kemerink, Molecular doping and trap filling in organic semiconductor host-guest systems, *J. Phys. Chem. C* **121**, 7767 (2017).
- [41] T. Upreti, Y. Wang, H. Zhang, D. Scheunemann, F. Gao, and M. Kemerink, Experimentally Validated Hopping-Transport Model for Energetically Disordered Organic Semiconductors, *Phys. Rev. Appl.* **12**, 064039 (2019).
- [42] A. Melianas, F. Etzold, T. J. Savenije, F. Laquai, O. Inganäs, and M. Kemerink, Photo-generated carriers lose energy during extraction from polymer-fullerene solar cells, *Nat. Commun.* **6**, 1 (2015).
- [43] N. Felekidis, A. Melianas, and M. Kemerink, Automated open-source software for charge transport analysis in single-carrier organic semiconductor diodes, *Org. electron. physics, Mater. Appl.* **61**, 318 (2018).
- [44] S. Wilken, T. Upreti, A. Melianas, S. Dahlström, G. Persson, E. Olsson, R. Österbacka, and M. Kemerink, Experimentally calibrated kinetic monte carlo model reproduces organic solar cell current-voltage curve, *Sol. RRL* **4**, 2000029 (2020).
- [45] L. Zhu, M. Zhang, G. Zhou, T. Hao, J. Xu, J. Wang, C. Qiu, N. Prine, J. Ali, W. Feng, X. Gu, Z. Ma, Z. Tang, H. Zhu, L. Ying, Y. Zhang, and F. Liu, Efficient organic solar cell with 16.88% efficiency enabled by refined acceptor crystallization and morphology with improved charge transfer and transport properties, *Adv. Energy Mater.* **10**, 1904234 (2020).
- [46] J. Wu, J. Lee, Y.-C. Chin, H. Yao, H. Cha, J. Luke, J. Hou, J.-S. Kim, and J. R. Durrant, Exceptionally low charge trapping enables highly efficient organic bulk heterojunction solar cells, *Energy Environ. Sci.* **13**, 2422 (2020).
- [47] J. Kniepert, A. Paulke, L. Perdígón-Toro, J. Kurpiers, H. Zhang, F. Gao, J. Yuan, Y. Zou, V. M. Le Corre, L. J. A. Koster, and D. Neher, Reliability of charge carrier recombination data determined with charge extraction methods, *J. Appl. Phys.* **126**, 205501 (2019).
- [48] W. Gong, M. A. Faist, N. J. Ekins-Daukes, Z. Xu, D. D. C. Bradley, J. Nelson, and T. Kirchartz, Influence of energetic disorder on electroluminescence emission in polymer: Fullerene solar cells, *Phys. Rev. B - Condens. Matter Mater. Phys.* **86**, 1 (2012).
- [49] S. N. Hood and I. Kassal, Entropy and disorder enable charge separation in organic solar cells, *J. Phys. Chem. Lett.* **7**, 4495 (2016).
- [50] S. Athanasopoulos, H. Bässler, and A. Köhler, Disorder vs delocalization: Which is more advantageous for high-efficiency organic solar cells?, *J. Phys. Chem. Lett.* **10**, 7107 (2019).
- [51] A. Melianas, V. Pranculis, A. Devižis, V. Gulbinas, O. Inganäs, and M. Kemerink, Dispersion-dominated photocurrent in polymer:Fullerene solar cells, *Adv. Funct. Mater.* **24**, 4507 (2014).
- [52] J. I. Khan, M. A. Alamoudi, N. Chaturvedi, R. S. Ashraf, M. N. Nabi, A. Markina, W. Liu, T. A. Dela Peña, W. Zhang, O. Alévêque, G. T. Harrison, W. Alsufyani, E. Levillain, S. De Wolf, D. Andrienko, I. McCulloch, and F. Laquai, Impact of acceptor quadrupole moment on charge generation and recombination in blends of IDT-based non-fullerene acceptors with PCE10 as donor polymer, *Adv. Energy Mater.* **11**, 2100839 (2021).
- [53] J. Kurpiers, T. Ferron, S. Roland, M. Jakoby, T. Thiede, F. Jaiser, S. Albrecht, S. Janietz, B. A. Collins, I. A. Howard, and D. Neher, Probing the pathways of free charge generation in organic bulk heterojunction solar cells, *Nat. Commun.* **9**, 2038 (2018).
- [54] N. R. Tummala, S. Mehraeen, Y. T. Fu, C. Risko, and J. L. Brédas, Materials-scale implications of solvent and temperature on [6,6]-phenyl-C61-butyric acid methyl ester (PCBM): A theoretical perspective, *Adv. Funct. Mater.* **23**, 5800 (2013).
- [55] N. R. Tummala, Z. Zheng, S. G. Aziz, V. Coropceanu, and J. L. Brédas, Static and dynamic energetic disorders in the C60, PC61BM, C70, and PC71BM fullerenes, *J. Phys. Chem. Lett.* **6**, 3657 (2015).
- [56] J. C. Aguirre, C. Arntsen, S. Hernandez, R. Huber, A. M. Nardes, M. Halim, D. Kilbride, Y. Rubin, S. H. Tolbert, N. Kopidakis, B. J. Schwartz, and D. Neuhauser, Understanding local and macroscopic electron mobilities in the fullerene network of conjugated polymer-based solar cells: Time-resolved microwave conductivity and theory, *Adv. Funct. Mater.* **24**, 784 (2014).
- [57] L. Perdígón-Toro, H. Zhang, A. Markina, J. Yuan, S. M. Hosseini, C. M. Wolff, G. Zuo, M. Stolterfoht, Y. Zou, F.

- Gao, D. Andrienko, S. Shoaee, and D. Neher, Barrierless free charge generation in the high-performance PM6:Y6 bulk heterojunction non-fullerene solar cell, *Adv. Mater.* **32**, 1906763 (2020).
- [58] J. Yuan, *et al.*, Understanding energetic disorder in electron-deficient-core-based non-fullerene solar cells, *Sci. China Chem.* **63**, 1159 (2020).
- [59] S. M. Hosseini, N. Tokmoldin, Y. W. Lee, Y. Zou, H. Y. Woo, D. Neher, and S. Shoaee, Putting order into PM6:Y6 solar cells to reduce the Langevin recombination in 400 nm thick junction, *Sol. RRL* **4**, 2000498 (2020).
- [60] S. M. Hosseini, S. Roland, J. Kurpiers, Z. Chen, K. Zhang, F. Huang, A. Armin, D. Neher, and S. Shoaee, Impact of bimolecular recombination on the fill factor of fullerene and nonfullerene-based solar cells: A comparative study of charge generation and extraction, *J. Phys. Chem. C* **123**, 6823 (2019).
- [61] A. Karki, J. Vollbrecht, A. L. Dixon, N. Schopp, M. Schrock, G. N. M. Reddy, and T. Nguyen, Understanding the high performance of over 15% efficiency in single-junction bulk heterojunction organic solar cells, *Adv. Mater.* **31**, 1903868 (2019).
- [62] A. Karki, J. Vollbrecht, A. J. Gillett, S. S. Xiao, Y. Yang, Z. Peng, N. Schopp, A. L. Dixon, S. Yoon, M. Schrock, H. Ade, G. N. M. Reddy, R. H. Friend, and T.-Q. Nguyen, The role of bulk and interfacial morphology in charge generation, recombination, and extraction in non-fullerene acceptor organic solar cells, *Energy Environ. Sci.* **13**, 3679 (2020).
- [63] J. I. Khan, R. S. Ashraf, M. A. Alamoudi, M. N. Nabi, H. N. Mohammed, A. Wadsworth, Y. Firdaus, W. Zhang, T. D. Anthopoulos, I. McCulloch, and F. Laquai, P3HT molecular weight determines the performance of P3HT:O-IDTBR solar cells, *Sol. RRL* **3**, 1900023 (2019).
- [64] W. Kaiser and A. Gagliardi, Kinetic monte carlo study of the role of the energetic disorder on the open-circuit voltage in polymer/fullerene solar cells, *J. Phys. Chem. Lett.* **10**, 6097 (2019).